Journal of Materials Chemistry A

Mechanistic Understanding of Electrochemical Plating and Stripping of Metal Electrodes

Journal:	*Journal of Materials Chemistry A*
Manuscript ID	TA-ART-11-2018-011326.R1
Article Type:	Paper
Date Submitted by the Author:	19-Jan-2019
Complete List of Authors:	Tewari, Deepti; Purdue University, School of Mechanical Engineering Mukherjee, Partha; Purdue University, School of Mechanical Engineering

Mechanistic Understanding of Electrochemical Plating and Stripping of Metal Electrodes

Deepti Tewari and Partha P. Mukherjee*

School of Mechanical Engineering, Purdue University, West Lafayette, IN 47907, USA

A revised manuscript submitted to

Journal of Materials Chemistry A

January, 2019

**Correspondence*: pmukherjee@purdue.edu (Partha P. Mukherjee)

Abstract

Lithium metal is an attractive negative electrode material for rechargeable lithium batteries because of its light weight and high electronegative redox potential. However, dendritic deposition of lithium during charging poses a safety concern. During discharging, some of the lithium may strip away from the electrode as the root of the dendrite is electrodissolved. This is referred to as dead lithium since it is not electrochemically active, which may result in low Coulombic efficiency. In this work, a comprehensive understanding of the interface evolution leading to the formation of dead lithium is presented based on a mechanism-driven probabilistic analysis. Non-dendritic interface morphology is obtained under reaction and ionic transport controlled scenarios. Otherwise, this may evolve into mossy, dendritic, whisker or needle-like structures with the main characteristic being the propensity for undesirable vertical growth. During discharging, pitted interface may be formed along with bulk dissolution. Surface diffusion is a key determinant controlling the extent of dead lithium formation, including a higher probability of the same when the effect of surface diffusion is comparable to that of ionic diffusion in the electrolyte and interface reaction.

Keywords: Metal anode, plating, stripping, dead lithium, mechanisms

Introduction

Rechargeable lithium batteries are ubiquitous in our technological society. They are used in electronic appliances, particularly cell phones, laptops, in transportation like hybrid vehicles, power sector and many other applications. Lithium-ion batteries have been a great commercial success. However, the graphite that acts as a host for intercalating Li is extra weight. Li is one of the lightest element (534 kg/m3) and has high redox potential (-3.04V vs SHE). The Li metal electrodes are promising because of lightweight and high energy density. The issue with Li metal anode is the propensity for dendritic morphology during charging which can cause short circuit and catastrophic failure. In addition, Li is consumed in creating solid electrolyte interphase on the newly created surface on dendrite. During discharging, there is detachment of some Li from the metallic electrode. This detached Li is referred to as dead Li since it is not electrochemically active. This dead Li reduces the Coulombic efficiency of the battery.

A continuum model was developed by Barton and Bockris[1] to study dendritic deposition on a metal substrate. A dendrite would grow faster because it would experience spherical diffusion compared to global linear diffusion. The surface tension was the driving force for dendrite propagation. Subsequently, Diggle *et al.*.[2] incorporated overpotential by using Butler-Volmer kinetic relation and Monroe and Newman[3] modeled dendritic growth between parallel electrodes with transient concentration and potential profiles. In all of these models, viscous and mechanical forces are not considered. Monroe and Newman[4] developed a model to include mechanical forces and its effect on exchange current densities and potentials at roughening interfaces. Another approach to model dendritic growth is through continuum phase field modeling[5].

Dissolution has been a topic of study in different fields like mineral dissolution[6–8], evolution of etch pits due to presence of screw dislocation and other defects[9,10], preferential etching of

crystallographic planes[11], particularly, etching of Silicon to create surface features[12,13]. The kinetics of reaction is influenced by local environment, for example, in the terrace-ledge-kink (TLK) model, reaction rates are different because of difference in the coordination number. Lasaga and Luttge proposed stepwave dissolution model, which describes both bulk dissolution and local etching of pits[14].

It is observed in Li metal electrodes that during discharging, some Lithium is detached from the electrode. Since it is electronically isolated, it does not participate in further electrochemical reaction and is called dead Li. Formation of dead Li is intrinsically linked to the nature of the electrodeposition during the previous charging cycle. Experimental studies[15–17] using TEM and SEM show that whiskers grow from root and since newly formed SEI is thinner and facilitates Li ion diffusion, during discharging, the roots of whiskers is dissolved at a faster rate leading to disconnection from the electrode. It can subsequently break away and float in the electrolyte or be connected to the electrode through the support of the SEI layer. Gireaud *et al.*[18] observed that dendrites originated on the pits formed during the discharge cycle. Several studies [19–21] by Dasgupata research group have correlated the voltage profile with the morphology of deposition or dissolution of Li symmetric cells with cycling. They attributed the change from peaking voltage profile during initial cycling to arcing voltage profile towards the end of cycling to the gradual buildup of dead Li. Aryanfar *et al.*[22] quantified the amount of dead Li based on images of electrode and dead Li during discharging and concluded that amount of dead Li is reduced if the cycling period is shortened. Yoon *et al.*[23] studied the continuum behavior of plating and stripping of Li metal and found that the amount of dead Li is less when the discharge rate is high.

Kinetic Monte Carlo (KMC) is a statistical technique and it is particularly useful in studying the morphology during deposition or dissolution. Shvab *et al.*[24] studied different precipitation

mechanism of nanoparticle aggregation. Trigueros *et al.*[25] studied diffusion controlled electrodeposition. Electrodeposition and associated morphology of the deposits were studied by Guo *et al.*[26] by specifying the relative probability of attachment of metal on the substrate or metal on metal. Drews *et al.*[27] and Liu[28] studied electrodeposition of copper and linked the reaction kinetics to the overpotential. KMC modeling was used to study plating on intercalation anode [29], formation of solid electrolyte interphase (SEI) [30], dendrite formation on metal anodes [31] and dendrite-SEI interactions [32]. Dissolution has also been studied by using KMC. Porous structures through dealloying were studied by Haldar[33] and Erlbacher[34]. KMC was used to investigate the surface roughness[11] and dissolution of crystal[35,36] and amorphous glass[37]. Since KMC can only resolve small length and time scales, multi-paradigm studies have used coupled KMC and continuum scale transport to bypass these limitations[38–40].

There are many applications[41] where controlled deposition or plating is achieved by electrodeposition, for example, thin coating of surface deposition in solar panels .There are also many instances where stripping or electrodissolution is used to obtain the desired feature, for example etching of Silicon to obtain microchannel. The batteries are more challenging because of cyclic plating and stripping of an electrode. Therefore, studying plating and stripping in concert would give better understanding of the issues related to Li metal electrodes. In the current work, a generalized probability based KMC model has been developed to study plating and stripping during charging and discharging. The KMC model includes diffusion of metal ion, diffusion on metallic surface and reaction (reduction or oxidation). The KMC model allows for formation of dead metal during discharging. A wide variety of morphology of deposition is seen during charging. During discharging, a pitted electrode-electrolyte interface evolves along with steady bulk dissolution. Surface diffusion is key factor in the evolution of morphology. During charging,

mossy deposition is obtained due to surface diffusion. During discharging, greater amount of dead metal is formed when the probability of surface diffusion is commensurate with the probabilities of oxidation reaction and ion diffusion. Since in batteries, the probability of reaction can be changed through applied overpotential, charging at slow reduction kinetics and discharging at fast oxidation kinetics will result in flat deposition during charging and minimize the amount of dead metal formation during discharging.

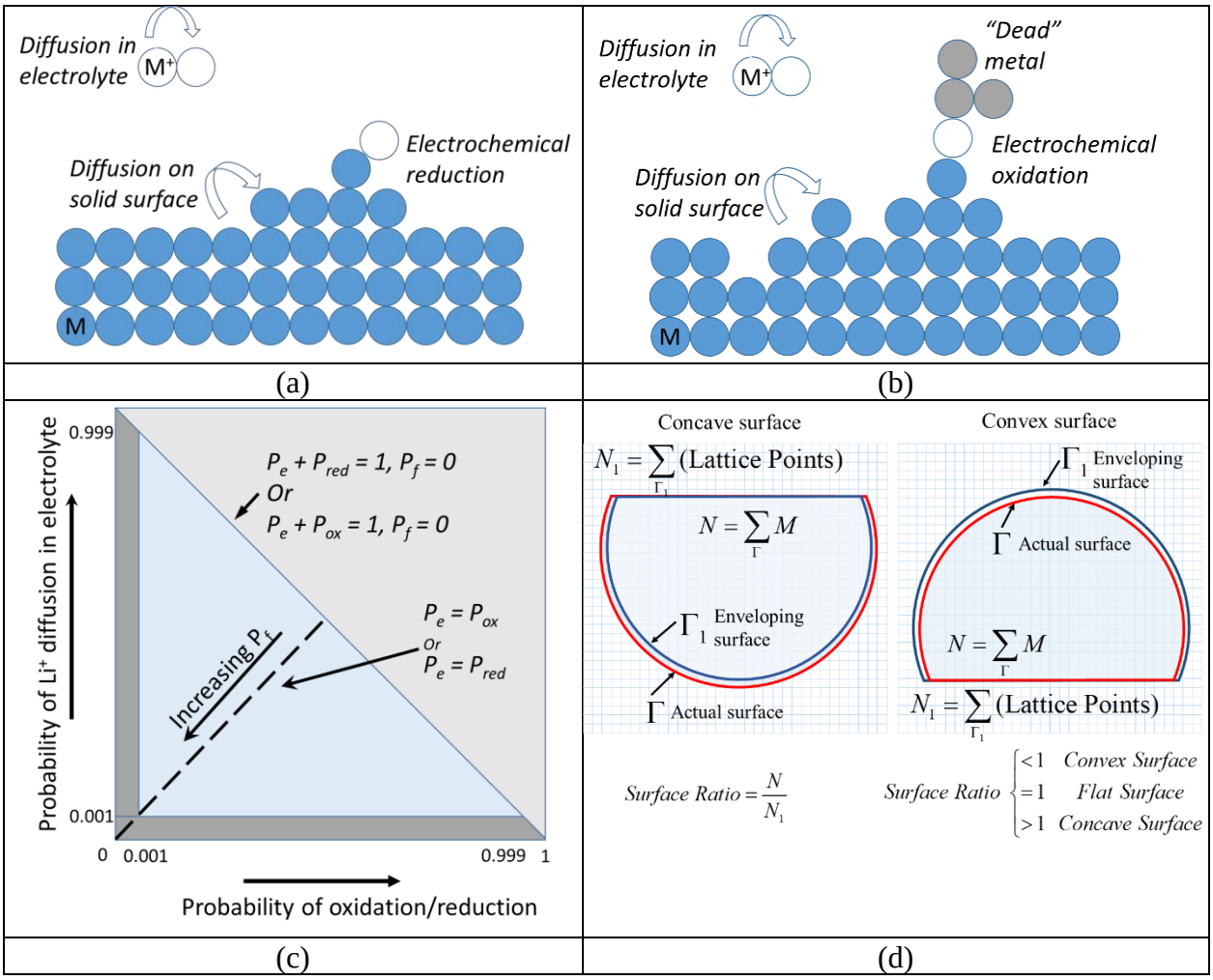

Figure 1: *Schematic of the KMC model* (a) transition events modeled in charging process (b) transition events for discharging process (c) probability space of transition events modeled during charging and discharging (d) determining surface ratio by counting N, number of metal atoms on the electrode surface and N_1, the number of lattice sites on the enveloping surface

Computational Model

A two dimensional lattice Kinetic Monte Carlo model was developed to model plating and stripping during charging and discharging process. During the charging process, following three events can occur as shown in Figure 1 (a)

(i) Diffusion of metal ion, M^+ in the liquid electrolyte

(ii) Electrochemical reduction of M^+ ion at the interface between electrode and electrolyte

(iii) Diffusion of metal atom M on the surface

During discharging, following three events are included in the KMC model as seen in Figure 1 (b)

(i) Diffusion of the metal ion, M^+ in the liquid electrolyte

(ii) Oxidation of metal atom on the interface between electrode and electrolyte

(iii) Diffusion of metal atom, M on the surface.

If a metal atom is the only connecting link between a group of atoms and the electrode and it is oxidized, the group of atoms become detached from the electrode as seen in Figure 1 (b). This group of atoms cannot participate in further electrochemical reactions and are referred to as “dead” metal.

The reaction rates of the three processes during charging and discharging are assigned directly in terms of probabilities of three processes included in the KMC model. During the charging process, P_{red} is the probability of reduction of M^+ ion at the interface, P_e is the probability of diffusion of M^+ ion in electrolyte and P_f is the probability of surface diffusion of M atom on surface. During discharging process, P_{ox} is the probability of oxidation of a metal atom in to M^+ ion. P_e and P_f have the same definition as charging. Figure 1 (c) shows the probability space

used in the KMC simulations. Since P_e and P_{red} or P_{ox} have to be non-zero for charging or discharging to occur, the minimum value for P_{red}/P_{ox} and P_e is 0.001. The maximum value that P_e and P_{red}/P_{ox} can take is 0.999. Since sum of probabilities is 1, P_f is not independent. The diagonal line shown in Figure 1 (c) is $P_e+P_{red}=1$ for charging or $P_e+P_{ox}=1$ for discharging and surface diffusion P_f is zero. The dotted line shown is for $P_e=P_{red}$ or $P_e=P_{ox}$. Where the diagonal and dotted line intersect, $P_e=1/2$, P_{ox} or $P_{red}=1/2$ and $P_f=0$. Moving on the $P_e=P_{red}$ line towards origin, implies larger value of P_f. Therefore, the diagonal line is a limiting case where there is no surface diffusion and moving towards origin implies very large value of P_f. For example, at $P_e=0.001$, $P_{red}=0.001$, $P_f=0.998$.

The electrochemical reactions occur at the interface of electrode and electrolyte. With plating or stripping, the interface changes and so does the surface area. To characterize the surface area, count the number of metal atoms on the actual interface, N. Next, find the unique set of all the lattice points, which are first neighbor of the atoms belonging to the interface and not occupied by metal atoms. Let this surface be referred to as the enveloping surface. Let N_1 be the sum of all the points belonging to the enveloping surface.

Define

$$Surface\ Ratio = \frac{N}{N_1} \quad (1)$$

Figure 1 (d) shows the schematic of determining the surface ratio. Consider a concave surface, the actual surface is shown as red while the enveloping surface is shown in blue. Since the perimeter of the enveloping surface is smaller than the actual surface, the surface ratio is greater than one. On the other hand, for convex surface, the perimeter of the enveloping surface is

larger than the actual surface and hence the surface ration is less than one. For a flat surface, the length of actual interface and the enveloping surface are same and the surface ratio is 1. Surface ratio is a tool to characterize the overall nature of the interface during plating or stripping. During plating, the nucleation phase or whiskers deposition or dendritic deposition, perimeter of the enveloping surface is larger than the actual interface surface ratio would be less than 1. During discharging or stripping, the interface becomes pitted and the length of the enveloping surface is smaller than the actual surface and therefore, the surface ratio is greater than 1. In case of porosity, the surface ratio would be greater than one. Having information about the enveloping surface could be useful. If a reaction occurs at the interface, it will be when a site on the enveloping surface is occupied by the reacting agent. N_1 gives an estimate about the number of sites available for the reaction. Example, for catalytic activity, surface ratio < 1 would be preferred. Surface ratio provides information about how the interface surface is evolving with plating and stripping, and perhaps it could be useful in describing the updated reaction rate on interface in continuum descriptions.

Define following parameters for analyzing the results of KMC simulations

$No.\ of\ \ layers\ deposited = \frac{No.\ of\ \ reduction\ reactions}{N_x}$	(2)
$AverageHeight = \frac{\sum_{i=1}^{M} y_i}{M}$	(3)
$No.\ of\ \ layers\ dissolved = \frac{No.\ of\ \ oxidation\ reactions}{N_x}$	(4)
$No.\ of\ \ layers\ of\ "dead"\ metal = \frac{No.\ of\ \ "dead"\ metal\ atoms}{N_x}$	(5)

In equations 2, 4 and 5, N_x is the number of lattice points in the horizontal direction. To calculate average height in equation 3, y_i is the vertical distance from the bottom boundary and M is the total number of atoms in the deposit.

In the two-dimensional KMC model, a small segment of the electrode-electrolyte interface is modeled. The lattice grid is ($N_x \times N_y$) = 175×100 sites, where 175 lattice points are in the horizontal direction and 100 lattice points are in the vertical direction. Periodicity is enforced in the horizontal direction. During the charging process, the first layer is comprised of metal atoms on which further deposition occurs. This boundary at the bottom is fixed, no surface diffusion is allowed. At the beginning, the fraction of lattice sites occupied by M^+ ions is 0.1. As deposition progresses, whenever an ion is reduced, another ion is introduced at the top boundary, such that the number of M^+ ion remains constant during simulation. The M^+ ions at the top boundary cannot diffuse up in the vertical direction. During discharging process, at the beginning, there are 50 layers of stacked metal atoms. Ten percent of the empty lattice sites is occupied by M^+ ions. During dissolution, a metal atom is oxidized and an M^+ ion is introduced. When this happens, an ion is removed such that the total concentration of the metal ions remain constant during the course of simulation. The other boundaries are same as in the charging process. The details of the KMC algorithm is given in supporting information document.

Results and Discussion

Charging

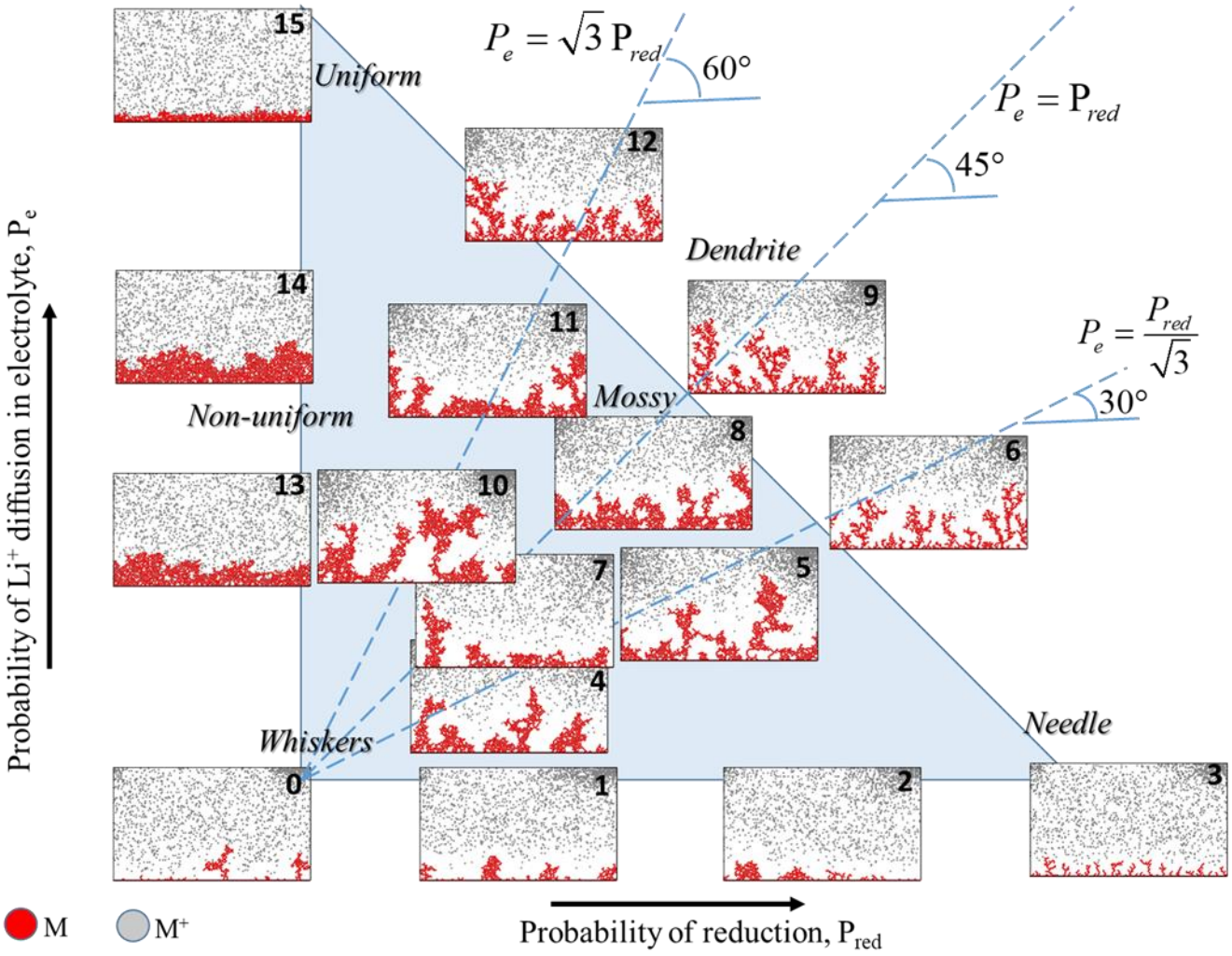

Figure 2: *Morphology of deposition during charging*. Pictures marked 0, 1, 2 and 3 use P_e=0.001 and P_{red} increasing from 0.001 to 0.999. Pictures labeled 0, 13, 14 and 15 use constant P_{red}= 0.001 and P_e increasing from 0.001 to 0.999. Pictures labeled 4, 5 and 6 lie on 30-degree line with respect to P_{red} axis. Pictures 7, 8 and 9 show the morphology for P_e=P_{red}. Pictures labeled 10, 11 and 12 lie on 60-degree line with respect to P_{red} axis. Pictures labeled 0, 1, 2, 3, 13, 14 and 15 are obtained at time 25000. Picture labeled 4 is at time 5000, 5 is at time 1500 and 6 is at 1500. Pictures labeled 7, 8 and 9 are obtained at time 2700, 2600 and 1500 respectively. Pictures labeled 10, 11 and 12 are obtained at time 4100, 2000 and 1500 respectively.

Dependence of morphology on reaction rate, ion diffusion and surface diffusion

The morphology of deposition for different probabilities of reduction reaction, P_{red}, surface diffusion, P_f and ion diffusion P_e is shown in Figure 2. Pictures labeled 0-3 lie on 0-degree line with respect to P_{red} axis with P_e=0.001. Pictures labeled 0,4,5,6 line on 30-degree line, pictures labeled 0,7,8,9 line on 45-degree line while pictures labeled 0,10,11,12 lie on 60-degree line with respect to P_{red} axis. Pictures labeled 0,13,14,15 line on 90-degree line with respect to P_{red} axis with P_{red}=0.001. All points are equally spaced on a line.

Consider pictures labeled 0-3. This is a diffusion control scenario, P_e is very small and the value of probability of reduction increases on moving along the P_{red} axis while probability of surface diffusion, P_f decreases. Since, the deposition is limited by the diffusion of ions to the metal surface, there is not much difference in terms of number of reduction reactions that occur with increasing value of Pred. However, the morphology of deposition changes from whiskers to needle like with increasing P_{red} and decreasing P_f. With greater probability of surface diffusion, there is rearrangement of metal atoms and the vertical realizations are favored because of access to metal ions. If surface diffusion is zero, newly reduced ions attach at the point of the metal surface where the reaction took place, which results in a fine needle deposition as seen in picture 3. Arakawa *et al.*[42] observed needle morphology of lithium deposition at high charge density.

Consider the 90-degree line with respect to P_{red} axis, where P_{red}=0.001. This is the reaction control region. Moving along this line, as P_e increases, P_f decreases. The deposition is limited by the number of reduction reaction that occur. When P_e is low and P_f is high, very few reactions occur and morphology is whiskers. As the probability of diffusion of ions, P_e increases, the morphology gradually changes from rough, non-uniform deposition to flat uniform deposit as seen in picture

labeled 15. Langenhuizen[43] reported that smooth deposition of lithium on Nickel substrate was obtained when the mass transport was increased by rotating electrodes.

On the diagonal line, $P_e+P_{red}=0$, the surface diffusion is zero. Pictures labeled 3,6,9,12 and 15 show the resulting morphology with zero surface diffusion. The morphology changes from needle like (picture 3) when the response limited by diffusion of ions to dendritic (picture 6,9,12) where P_e and P_{red} are comparable to uniform deposition (picture 15) where reaction kinetics determines the morphology.

The morphology of deposits is mossy in transition between these limiting scenarios. The morphology of the deposition is a complex interplay between probabilities of reaction, ion diffusion and surface diffusion. During charging, a flat surface or uniform deposition is desired. Uniform deposition is obtained only for very large probability of ion diffusion.

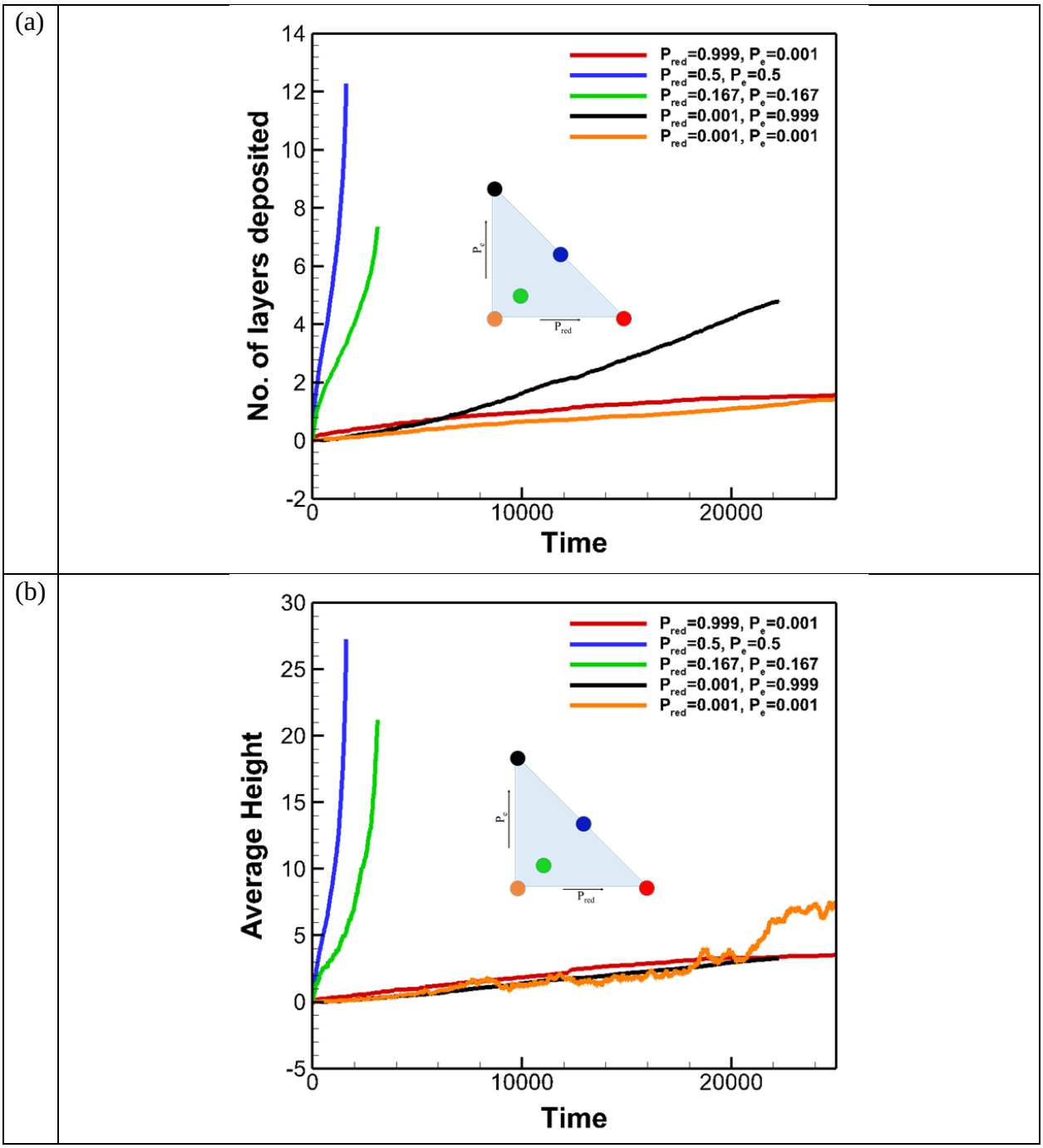

Figure 3: Plating as a function of time (a) Number of layers of metal atoms deposited due to reduction (b) Average height of deposition. The inset triangle shows the value of P_e and P_{red} on probability space for the five curves plotted.

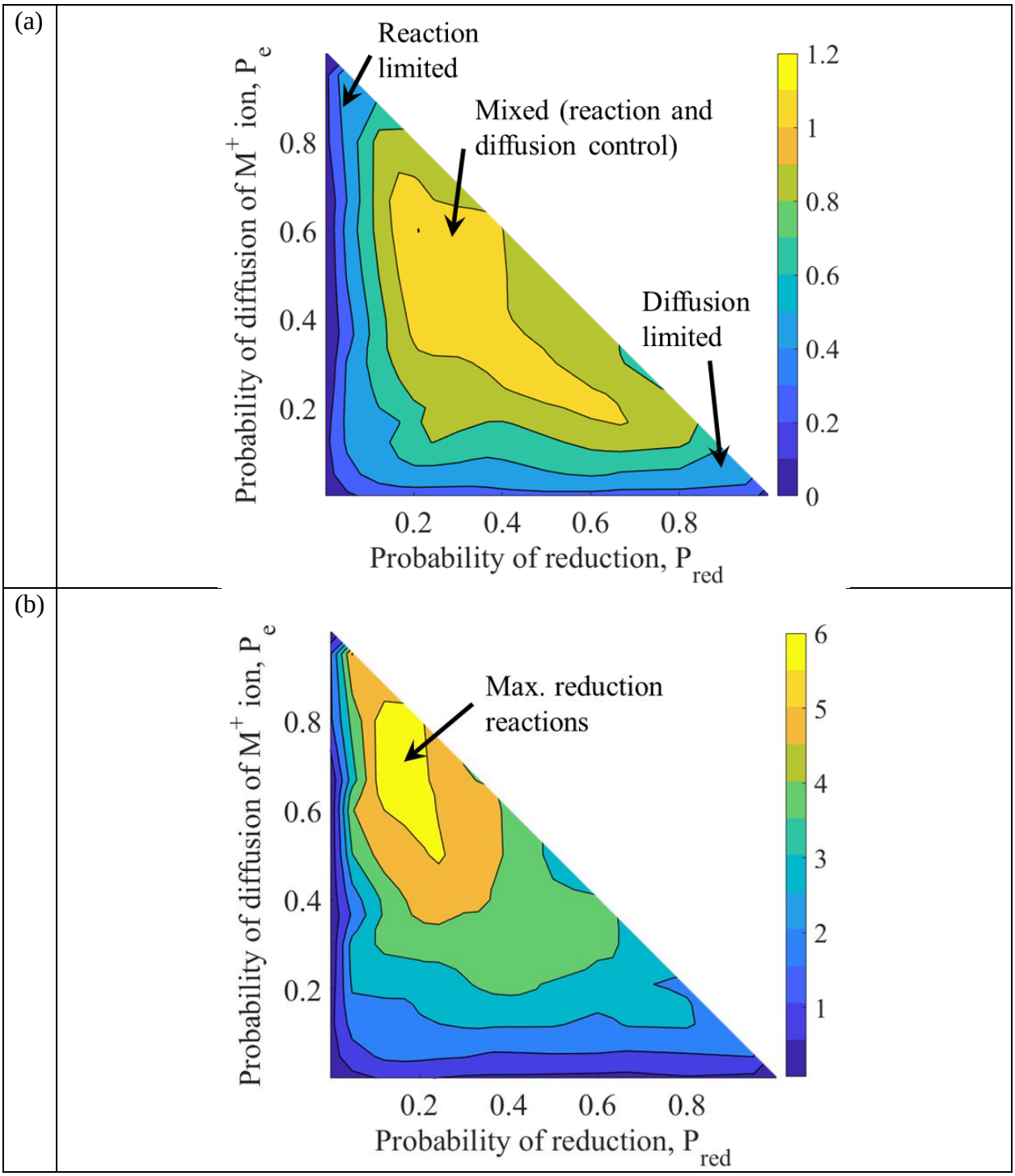

Figure 4: Contour of number of layers deposited with respect to probability of reduction, P_{red} and probability of diffusion of M^+ ion in electrolyte, P_e (a) at time = 100 (b) at time = 1250

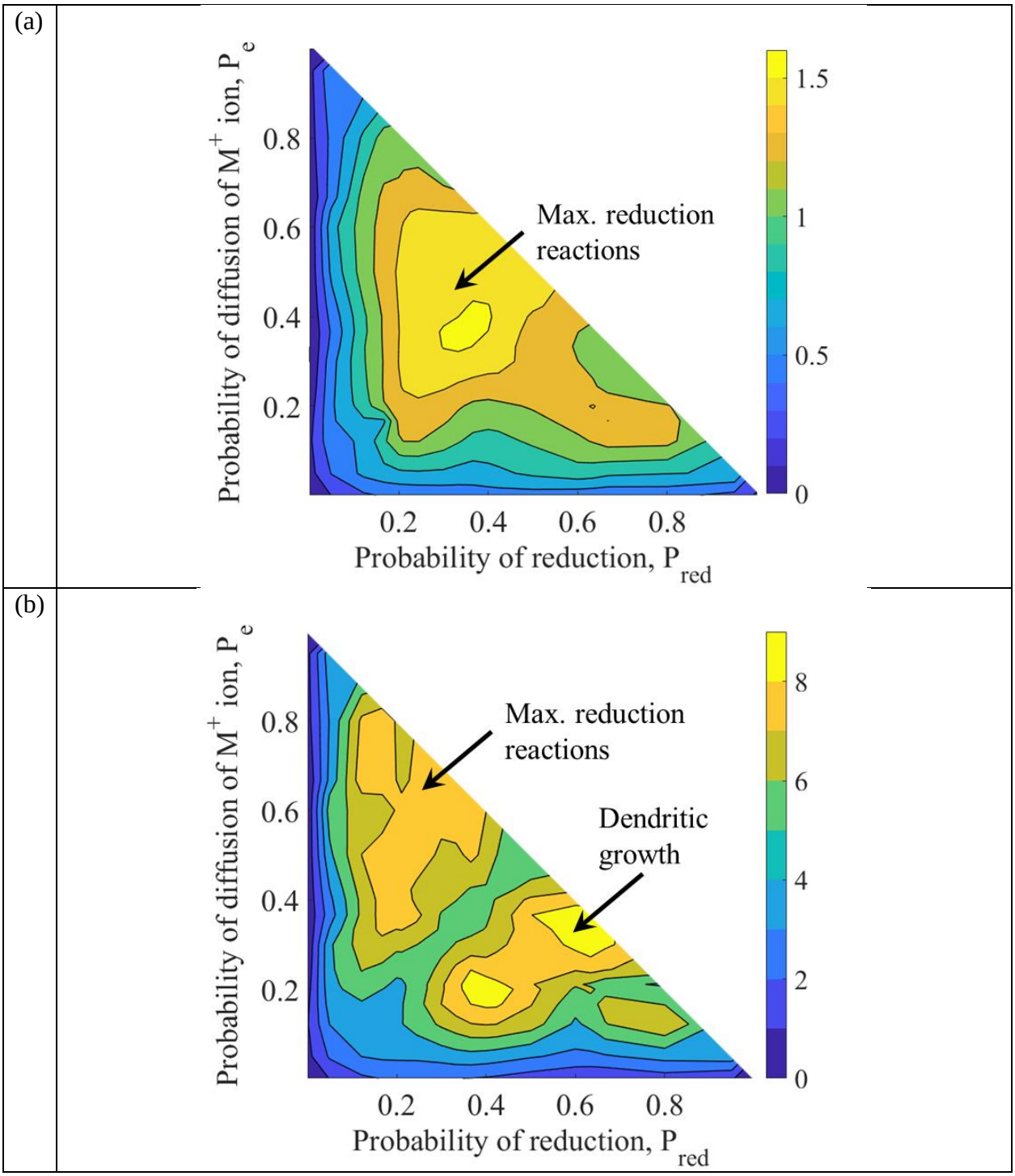

Figure 5: Contour of average height of deposition with respect to probability of reduction, P_{red} and probability of diffusion of M^+ ion in electrolyte, P_e (a) at time = 100 (b) at time = 1250

Number of layers and average height of deposition

The number of layers deposited on metal electrode is shown in Figure 3(a) as a function of time for five cases shown as dots on the probability space in the inset figure. The rate of deposition is nearly same for (P_{red}=0.999, P_e=0.001) and (P_{red}=0.001, P_e=0.000) even though the morphology is very different as seen in Figure 2. There are more layers deposited for higher ion diffusion (P_{red}=0.001, P_e=0.999). The fastest deposition occurred for P_e=P_{red}=0.5, with no surface diffusion. For both, P_{red}=P_e=0.167 and P_{red}=P_e=0.5, the slope of the curve of number of layers deposited with respect to time is very steep, indicating that likely dendritic deposition is occurring. However, the same information cannot be inferred form the other three curves.

The average height of the deposit with respect to time is shown in Figure 3(b) for five different cases as shown in the inset figure. The average height of the deposit increases very rapidly for P_{red}=P_e=0.5 and P_{red}=P_e=0.167 which is due to dendritic deposition. In figure 3(a) the number of layers deposited for P_{red}=0.001, P_e=0.009, black curve is larger than P_{red}=0.009, P_e=0.001, while in Figure 3(b) the average height of the deposit is same for both cases. For the black curve, the morphology of deposit is flat or uniform, while the red curve is for needle like deposit. So even though, more layers are deposited for P_{red}=0.001, P_e=0.009, the average height low compared to the needle like deposition for P_{red}=0.999, P_e=0.001 where fewer layers are deposited, but the average height is relatively larger. The average height for P_{red}=0.001, P_e=0.001 increases after time=20,000. Even though, the number of layers deposited is same as P_{red}=0.999, P_e=0.001. The morphology is whisker like and because of very high surface diffusion; the average height fluctuates and increases after some time due to rearrangements of atoms in the vertical direction. An important point to note is the different time scales of deposition for different kind of

morphology. For dendritic and mossy morphology, where P_{red} and P_e are both high and are of the same order, the time before number of layers of deposition grow very rapidly is ~10^3, while for extreme cases, when the deposition is constrained by reduction reaction or ion diffusion, the time to observe the morphology is 10^4 or larger.

Figure 4 (a) and (b) shows the contour plot of number of layers deposited with respect to probability of reduction, P_{red} and probability of diffusion of ion, P_e at time =100 and time=1250 respectively. At time=100, fewer layers are deposited when either the probability of reduction reaction, P_{red} is very small (marked as reaction limited in Figure 4(a)) or the probability of diffusion of ions, P_e is very small (marked as diffusion limited). In the mixed region, where diffusion of ions and reaction are in play, maximum number of reduction events occur and the number of layers deposited is highest. However as deposition progresses, the region in probability in which the maximum number of reduction reactions and hence the highest number of layers deposited moves up as seen in Figure 4(b). The highest number of reactions occur when P_e/P_{red} is larger than 2.

The contour plot of average height of deposition with respect to probability of reduction, P_{red} and probability of ion diffusion, P_e at time=100 and time=1250 is shown in Figure 5 (a) and (b) respectively. The average height is very small in diffusion limited and reaction limited regions. In Figure 5 (a), the average height is maximum for mixed (reaction and diffusion control) region and this corresponds to the largest number of reduction reaction occurring as seen Figure 4(a). However at time =1250, there are two distinct regions for which the average height of deposition is large as seen Figure 5(b). The region corresponding to larger P_{red} and smaller P_e (P_e/P_{red} <1), has greater value for average height of deposit because of nature of morphology. Dendrites are formed for these combinations of P_{red} and P_e as seen from Figure 2. The region corresponding to $P_{red}<P_e$

(P_e/P_{red}>1) has greater value of average height because maximum number of reduction reactions occur in that region as seen in Figure 4(b).

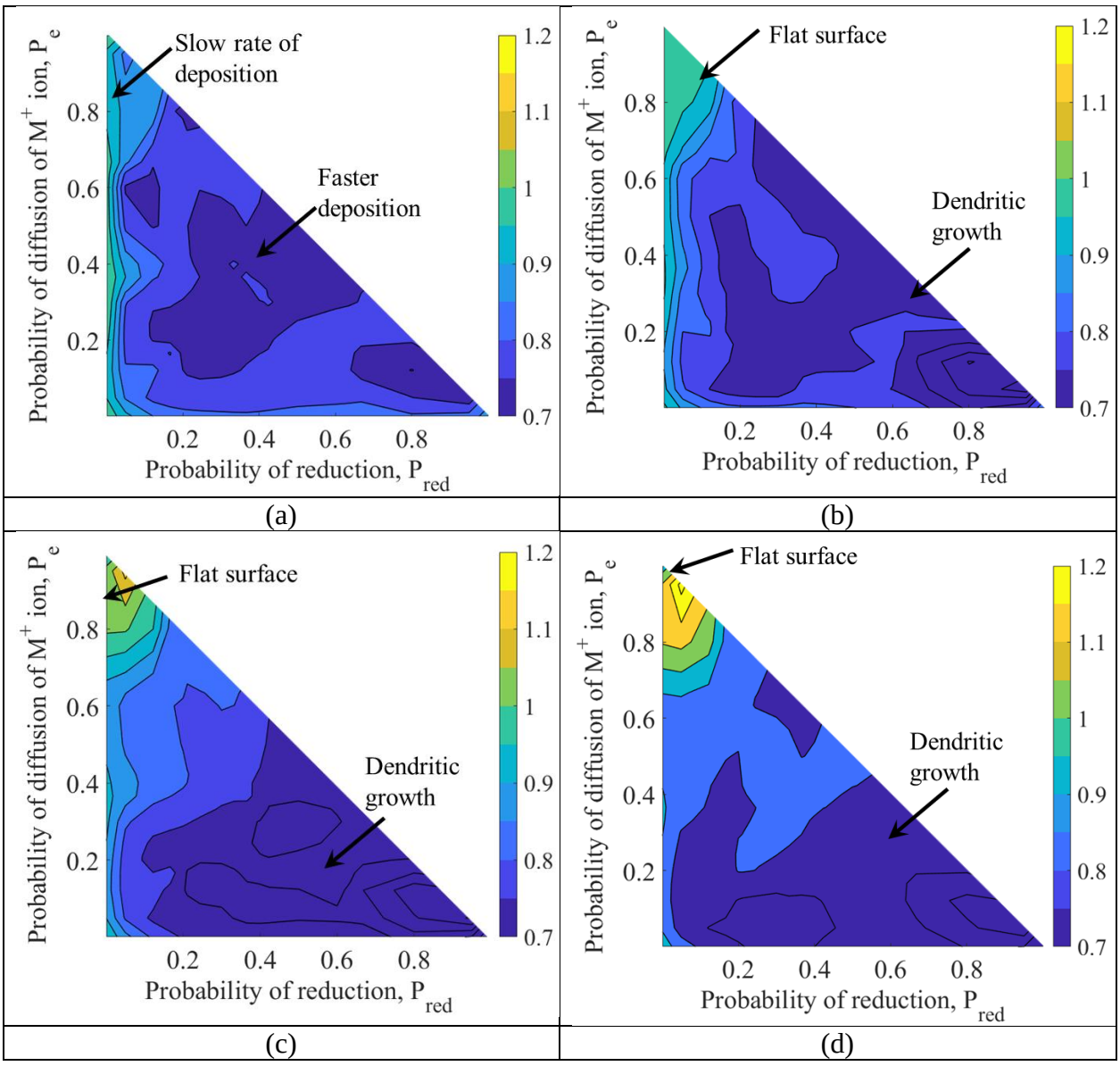

Figure 6: Contour of surface ratio of the interface between electrode and electrolyte with respect to probability of reduction, P_{red} and probability of diffusion of M^+ ion in electrolyte, P_e (a) at time = 100 (b) at time = 500 (c) at time = 750 (d) at time = 1250

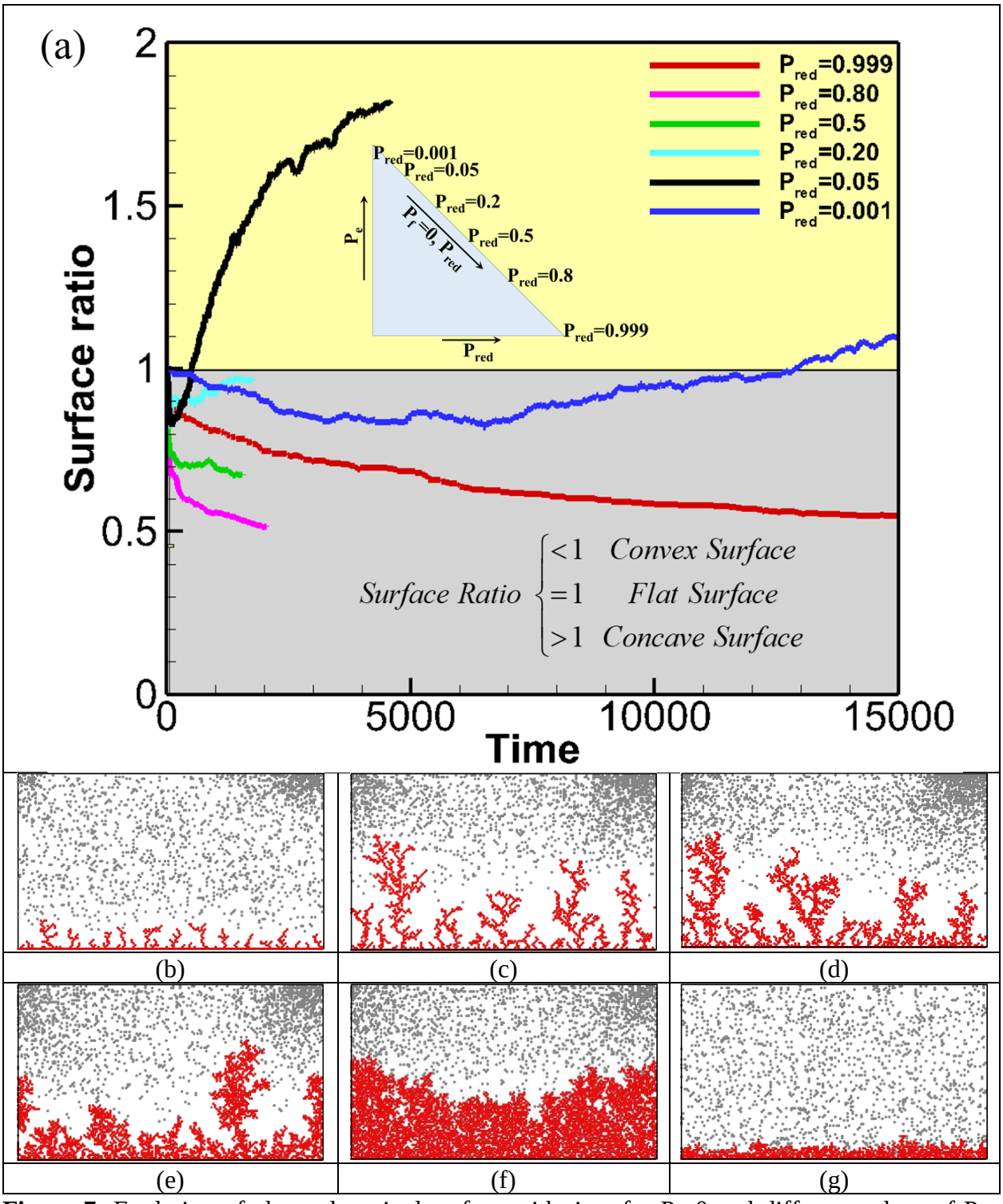

Figure 7: Evolution of electrodeposited surface with time for P_f=0 and different values of P_{red} (P_e=1-P_{red}). (a) Surface ratio (b) Microstructure for P_{red} = 0.9999 at time = 25000 (c) Microstructure for P_{red} = 0.8 at time = 2000 (d) Microstructure for P_{red} = 0.5 at time = 1500 (e) Microstructure for P_{red} = 0.2 at time = 1700 (f) Microstructure for P_{red} = 0.05 at time = 4500 (g) Microstructure for P_{red} = 0.001 at time = 25000

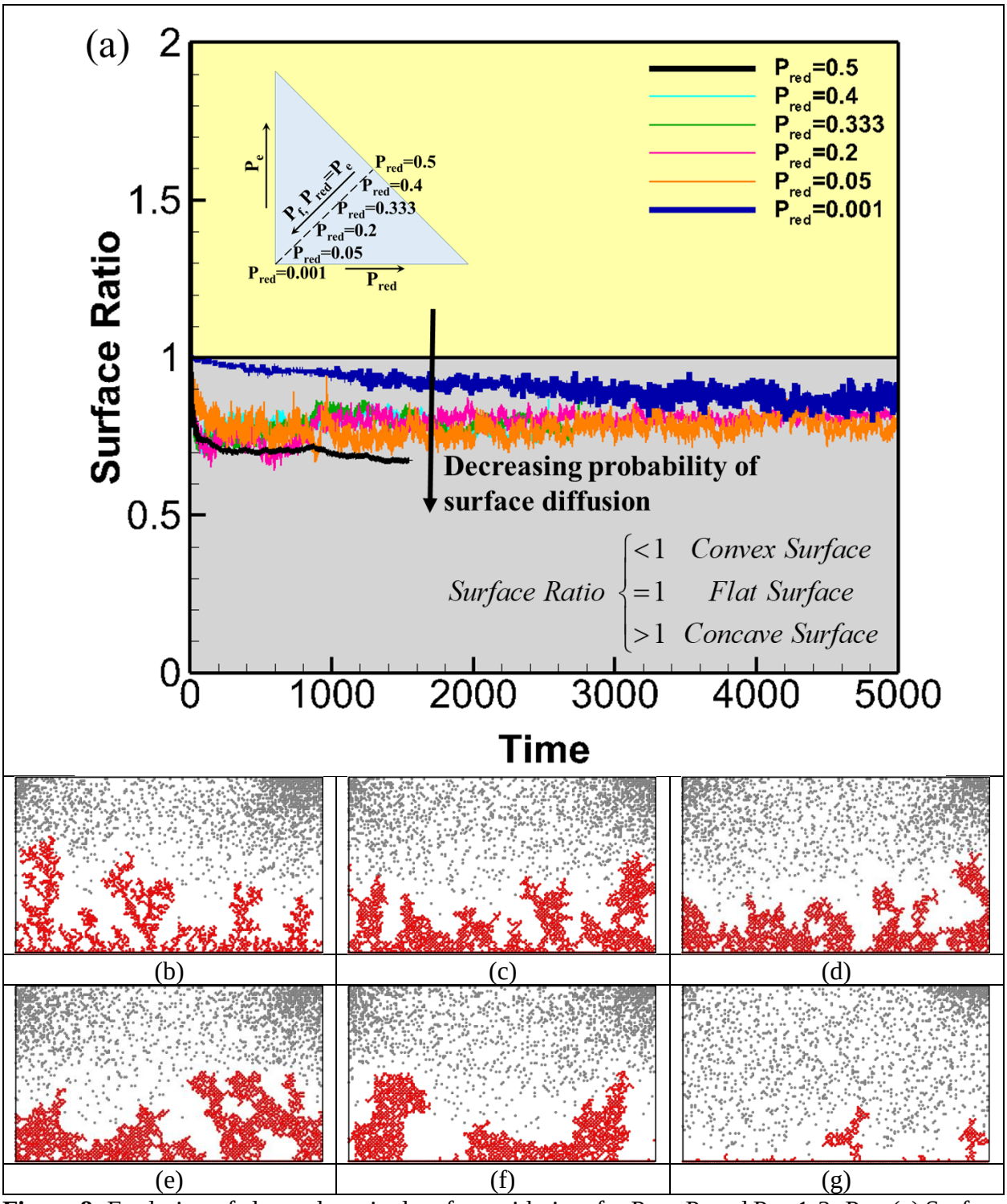

Figure 8: Evolution of electrodeposited surface with time for $P_{red}=P_e$ and $P_f = 1-2\times P_{red}$. (a) Surface ratio (b) Microstructure for $P_{red}=P_e=0.5$ at time=1500 (c) Microstructure for $P_{red}=P_e=0.4$ at time=2300 (d) Microstructure for $P_{red}=P_e=0.3333$ at time=2600 (e) Microstructure for $P_{red}=P_e=0.2$ at time=5000 (f) Microstructure for $P_{red}= P_e=0.05$ at time=15000 (g) Microstructure for $P_{red} = P_e =0.001$ at time=25000

Evolution of surface formed at the interface between electrode and electrolyte

The contour plots of surface ratio with respect to probability of reduction, P_{red} and probability of diffusion of M^+ ions, P_e at time = 100, 500, 750 and 1250 is shown in Figure 6 (a) to (d). At time 100, across the entire P_{red}-P_e space, the surface ratio is less than one. In the reaction-controlled region, the surface ratio is close to 1 because the interface is nearly flat due to very few reduction reactions. In the mixed reaction and diffusion regime, there are more layers deposited and the surface ratio is lowest. In Figure 6 (b), the surface ratio is 1 for very high ion diffusion in electrolyte and small reaction rates. In (c), at the very tip, where P_e is 0.999, the interface is flat, however at slightly larger values of P_{red}, the surface ratio is greater than 1 indicating rough deposit. Meanwhile, the surface ratio is less than 1 for majority of space. In (d), the region in which surface ratio is greater than 1 has grown, For larger reaction rates, more rough deposition occurs while at the very tip, the surface ratio is 1. It is important to note that there is transition in the value of surface ratio in the region of uniform deposition, from slightly less than one to greater than one. In the region where there is dendritic growth, there is not significant change in the value of surface ratio. Flat or uniform deposition is obtained when ion diffusion is about three orders of magnitude greater than reaction rate.

Figure 7 shows the evolution of surface ratio and the corresponding morphology for different reaction rates P_{red} and ion diffusion P_e combinations and probability of surface diffusion is zero. The inset picture in Figure 7 (a) shows that value of P_{red} ranging from 0.001 to 0.999 on the diagonal line with no surface diffusion. Figure 7 (b)-(g) show the corresponding morphology. While the value of P_{red} decreases from 0.999 to 0.001, the value of P_e increases from 0.001 to 0.999. From (b) to (g), the trend goes from needle like deposit to dendritic to more bushy branch like deposit to rough deposit with pores to more uniform deposit. One common feature for the

surface ratio curves is that all of them have value less than one (due to nucleation, which is a convex geometric feature). For P_{red}=0.05 and 0.001, there is crossover from less than one to greater than one. For P_{red}=0.05, rate at which deposition occurs is faster and the crossover at smaller time. Since the morphology shows many pores, the value of surface ratio is high. For P_e=0.001, the crossover occurs after a very long time and the surface ratio is close to one. For other cases, surface ratio is less than one, although it approaches a steady value after some time.

Figure 8 shows the evolution of surface ratio for equal probability of reduction and ion diffusion (P_{red}=P_e) and the corresponding morphology. Surface diffusion increases from 0 at P_{red}=0.5 to 0.998 at P_{red}=0.001. The inset picture in Figure 8 (a) shows the values of P_{red} used on the P_{red}=P_e line. The surface ratio for the entire range of P_{red} is less than one, which is corroborated by the morphology of deposit shown in (b), to (g). The morphology changes from dendritic as seen in (b) when there is no surface diffusion to mossy (c)-(d), thick pillars (f) and whiskers (g) as P_{red} decreases and probability of surface diffusion increases. The surface ratio is lowest for zero surface diffusion and P_{red}=0.5 and highest for P_{red}=0.001. There are fluctuations in surface ratio when surface diffusion is allowed because of rearrangement to atoms on the surface.

The average surface at the interface is convex in nature when the morphology of deposition is any other than flat or non-uniform deposit. The envelope of the surface is about 2 times larger than actual surface for dendritic deposit. This might be useful in updating the surface activity term in the reaction rate calculations.

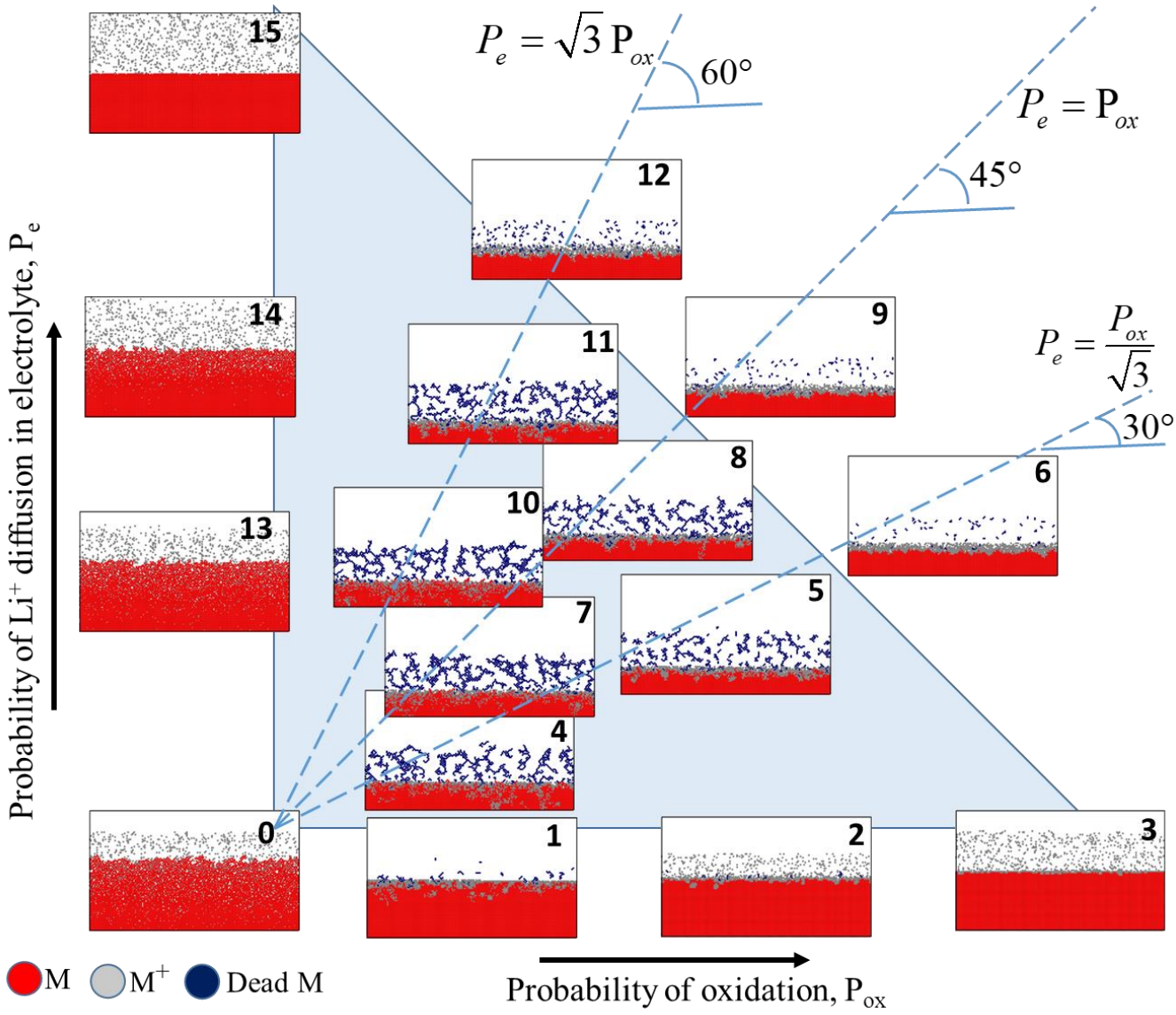

Figure 9: *Morphology during discharging*. Pictures marked 0, 1, 2 and 3 use P_e=0.001 and P_{ox} increasing from 0.001 to 0.999. Pictures labeled 0, 13, 14 and 15 use constant P_{ox}= 0.001 and P_e increasing from 0.001 to 0.999. Pictures labeled 4, 5 and 6 lie on 30-degree line with respect to P_{ox} axis. Pictures 7, 8 and 9 show the morphology for P_e=P_{ox}. Pictures labeled 10, 11 and 12 lie on 60-degree line with respect to P_{ox} axis. All the pictures are obtained at time=100.

Discharging

Dependence of morphology on reaction rate, ion diffusion and surface diffusion

The morphology of dissolution or stripping with different probabilities of oxidation, ion diffusion and surface diffusion is shown in Figure 9. The distribution of pictures marked 0 to 15 with respect to P_{ox} and P_e is same as described during charging. On 0-degree line with respect to P_{ox} axis, at very high P_{ox}, the layer is oxidized very quickly, but the diffusion of ions is so low that it acts as a kind of passivating layer and inhibits further reaction. In pictures labeled 1 and 2, some pits are formed and because of higher probability of surface diffusion, some of the electrolyte is trapped. Picture 0 shows a porous structure due to high frequency of surface diffusion and very few reactions.

On 90-degree line with respect to P_{ox} axis, very few oxidation reactions occur, and as probability of surface diffusion decreases, so does the porosity of the microstructure. Consider the diagonal line, where there is no surface diffusion, the interface between electrode and electrolyte look almost same for pictures 6, 9 and 12, however the amount of dead metal is higher for picture 12. This is the region of mixed control where reaction and ion diffusion are both important. If surface diffusion is allowed, the quantity of dead metal formed is significantly higher than zero surface diffusion. Surface diffusion is a critical factor that affects the amount of dead metal.

The mixed control region is where maximum dissolution of metal occurs. This is similar to charging process, where maximum deposition occurs in the mixed control regime. The dissolution results in pitted interface, however when probability of surface diffusion is high, there are trapped ions in some deeper pits. Pitting is observed on the lithium metal electrode surface during stripping [20,44]. Gireaud el al [18] observed pitting of the lithium electrode at both high and low current density. At high current density, the dissolution of lithium occurred along the slip planes [18]. It can be

concluded surface diffusion is a key parameter in reducing the amount of dead metal formed. When the ion diffusion is slow, there is high concentration of ions near the interface.

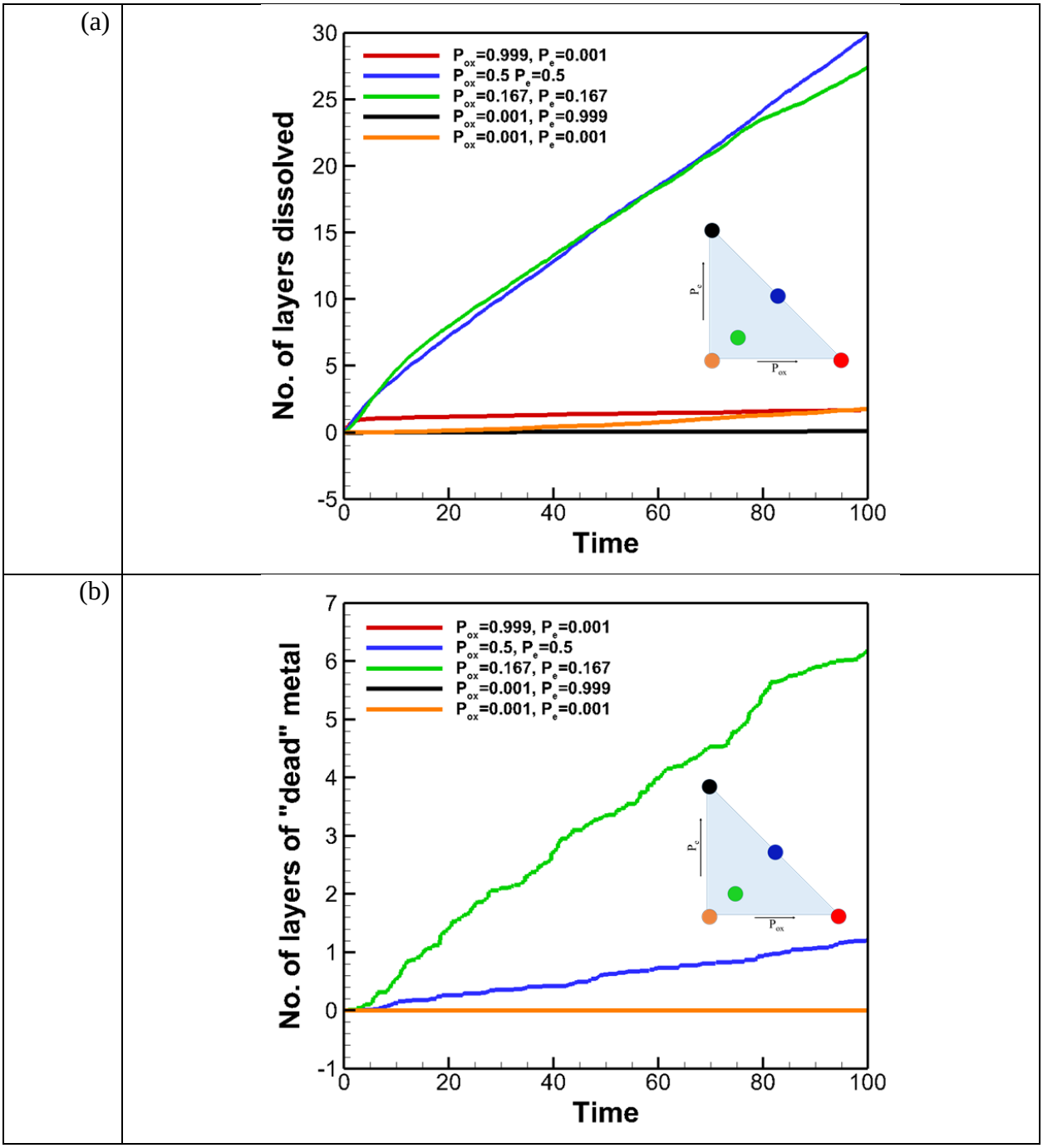

Figure 10: *Striping as a function of time* (a) Number of layers of metal dissolved due to oxidation reactions (b) Number of layers of "dead" metal. The inset triangle shows the value of P_e and P_{ox} on probability space for the five curves plotted.

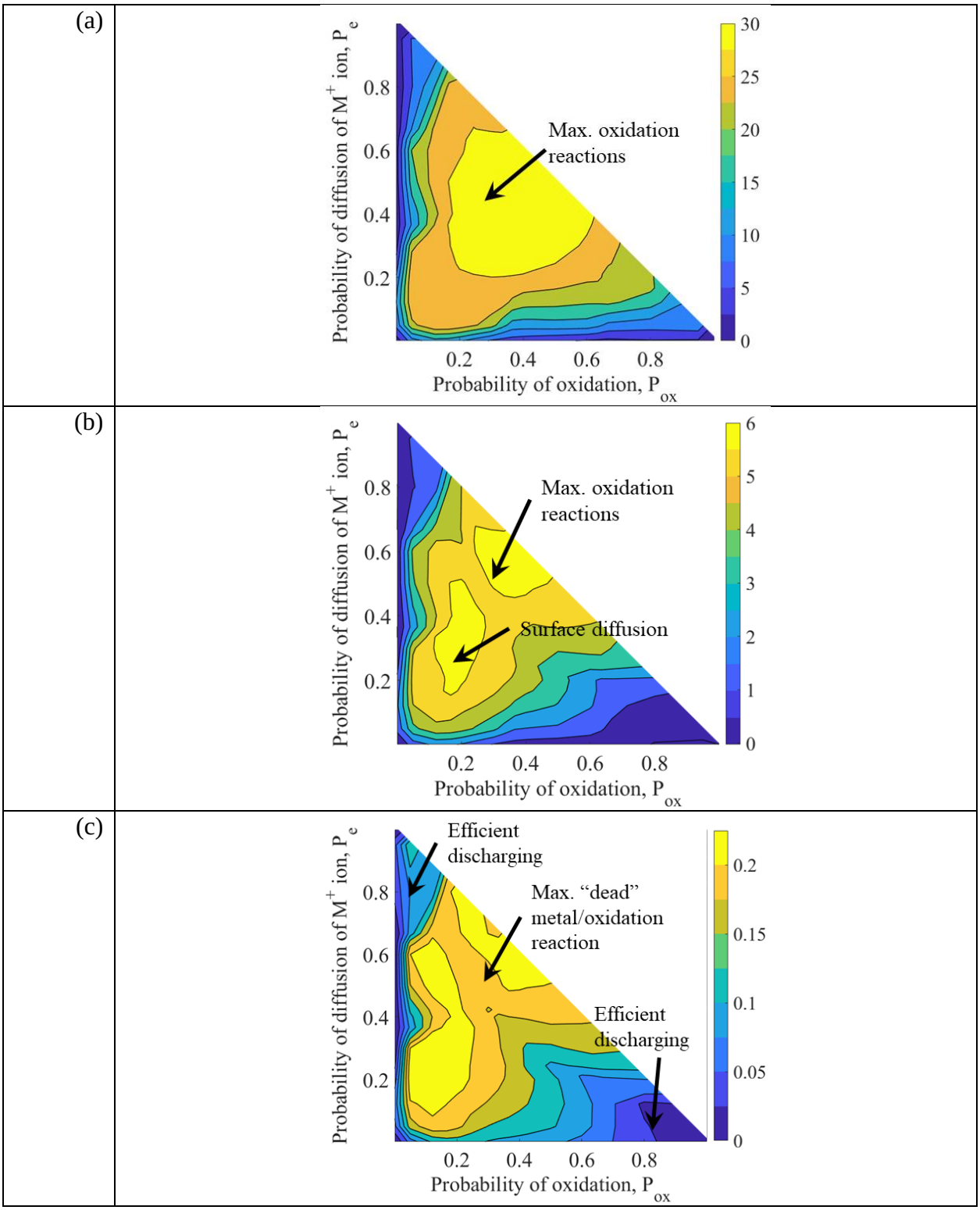

Figure 11: Contours with respect to probability of oxidation, P_{ox} and probability of diffusion of M^+ ion in electrolyte at time=100. (a) Number of layers dissolved (b) Number of layers of "dead" metal (c) ratio of "dead" metal and number of oxidation events

Number of layers dissolved and layers of "dead" metal

Figure 10 shows the number of layers dissolved and number of layers of "dead" metal formed during the discharging process. The inset picture marks the five (P_{ox},P_e) pairs as dots on input probability space. In Figure 10 (a), the number of layers dissolved is same for two cases when $P_{ox}=P_e=0.5$ and $P_{ox}=P_e=0.167$. Very few layers are dissolved when the system is constrained by either diffusion or oxidation reactions. The number of layers dissolved is linear with time for all five cases, although the slope vary. This is in contrast to the charging process, when number of layers deposited rose very sharply when (P_{ox},P_e) was equal to (0.5,0.5) and (0.167,0.167) respectively. When $P_{ox}=0.999$ and Pe=0.001, the number of layers dissolved is 1 and it is same throughout the discharge process. The ions formed during discharge cover the interface due to slow ionic diffusion and act as a passivating layer.

Figure 10 (b) shows the number of layers of dead "metal" with time. For the three cases, where P_e or P_{ox} or both of them are very low (the three corner points on the inset picture), no "dead" metal is formed. The number of layers of dead metal increases linearly with time indicating that cluster of atoms are detaching from electrode as the oxidation progresses. Almost five times more dead metal is formed between blue and green curves. Between these two cases, surface diffusion is the differentiating factor. With surface diffusion, rearrangement of atoms lead to situations where an atom is the lynchpin between a group of atoms and the rest of the electrode. If this particular atom is oxidized, the group of atoms are electrically detached from the electrode and contribute to "dead" metal. Surface diffusion strongly affects the magnitude of "dead" metal formed during discharging. It has been experimentally observed that particulate like lithium deposits were uniformly stripped while needle like lithium deposits resulted in dead lithium [45]. Kushima et al [15]

observed the formation of dead lithium due to preferential dissolution of lithium whiskers at the root.

The contour plots of number of layers dissolved, the number of layers of dead metal formed and the ratio of number of dead metal and number of oxidation events with respect to probability of oxidation and probability of diffusion of ion in electrolyte is shown in Figure 11. In the diffusion limited and reaction-limited regions, very few layers are dissolved as seen in Figure 11 (a) while in the mixed control region, where both reaction and ion diffusion are equally likely, maximum number of layers are dissolved. The number of layers of dead metal formed is maximum in two regions. In one region, the maximum in dead metal coincides with the highest number of oxidation reactions in (a). In the other region of maximum dead metal results due to high surface diffusion despite fewer oxidation reactions in comparison. Figure 11 (c) shows the number of dead metal per oxidation reaction. The number of dead metal formed is about 20 percent of the total oxidation reactions in the mixed control region. For efficient discharge, high P_{ox} and low P_e or vice-versa is preferable. In lithium batteries, Coulombic efficiency measures the irreversible loss of cycling capacity. Formation of dead lithium leads to loss in Coulombic efficiency. The Coulombic efficiency of 80 percent to 90 percent for discharging is reported for lithium metal electrodes by Langenhuizen [43] while Steiger et al [16] report about 30 percent capacity loss due to undissolved lithium. Experimentally, the loss in Coulombic efficiency is due to loss of electroactive lithium as well as formation of solid electrolyte interphase (SEI) and other irreversible side reactions.

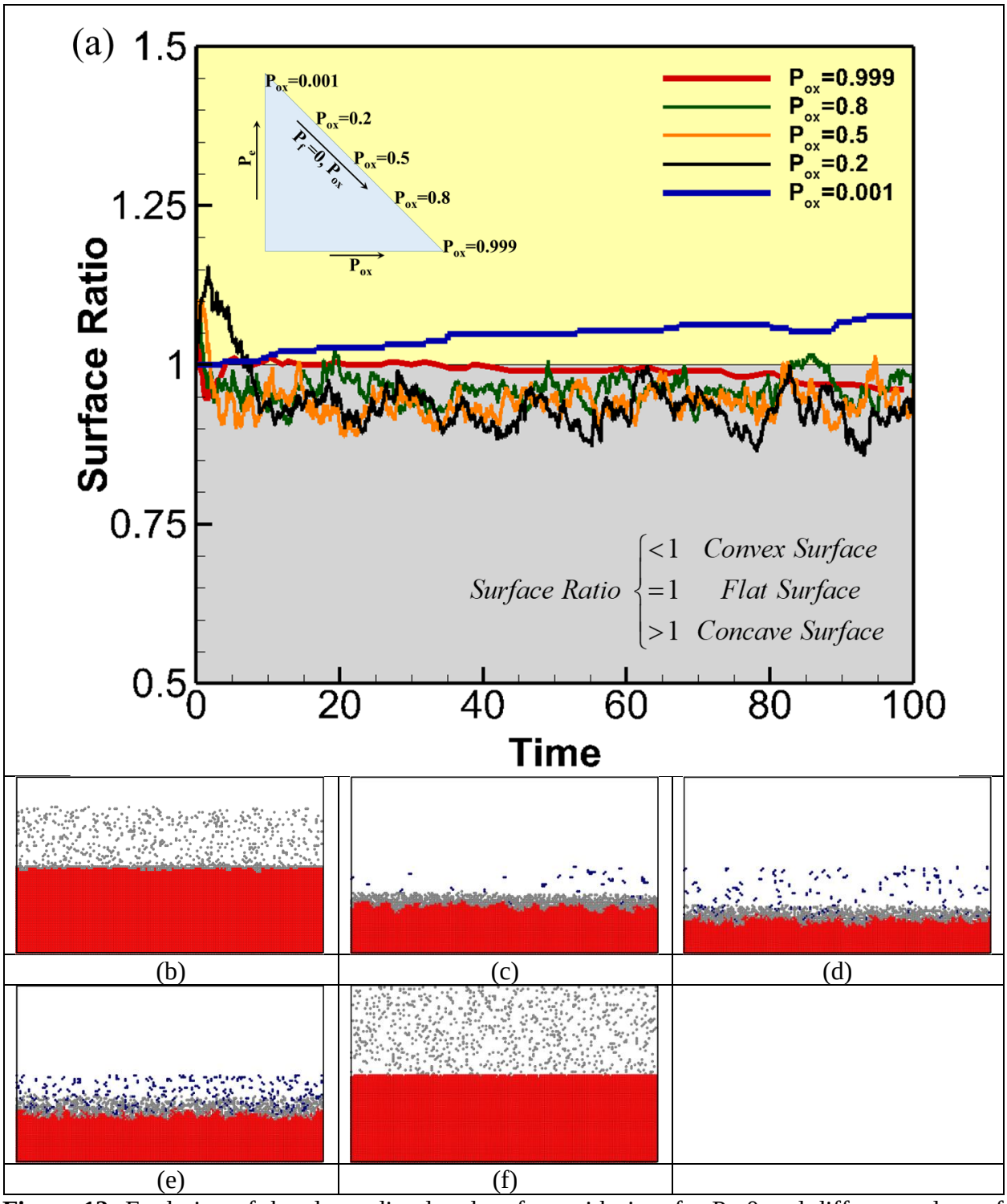

Figure 12: Evolution of the electrodissoluted surface with time for P_f=0 and different values of P_{ox}, (P_e=1-P_{ox}). (a) Surface ratio (b) Microstructure for P_{ox}=0.999 (c) Microstructure for P_{ox}=0.8 (d) Microstructure for P_{ox}=0.5 (e) Microstructure for P_{ox}=0.2 (f) Microstructure for P_{ox}=0.001

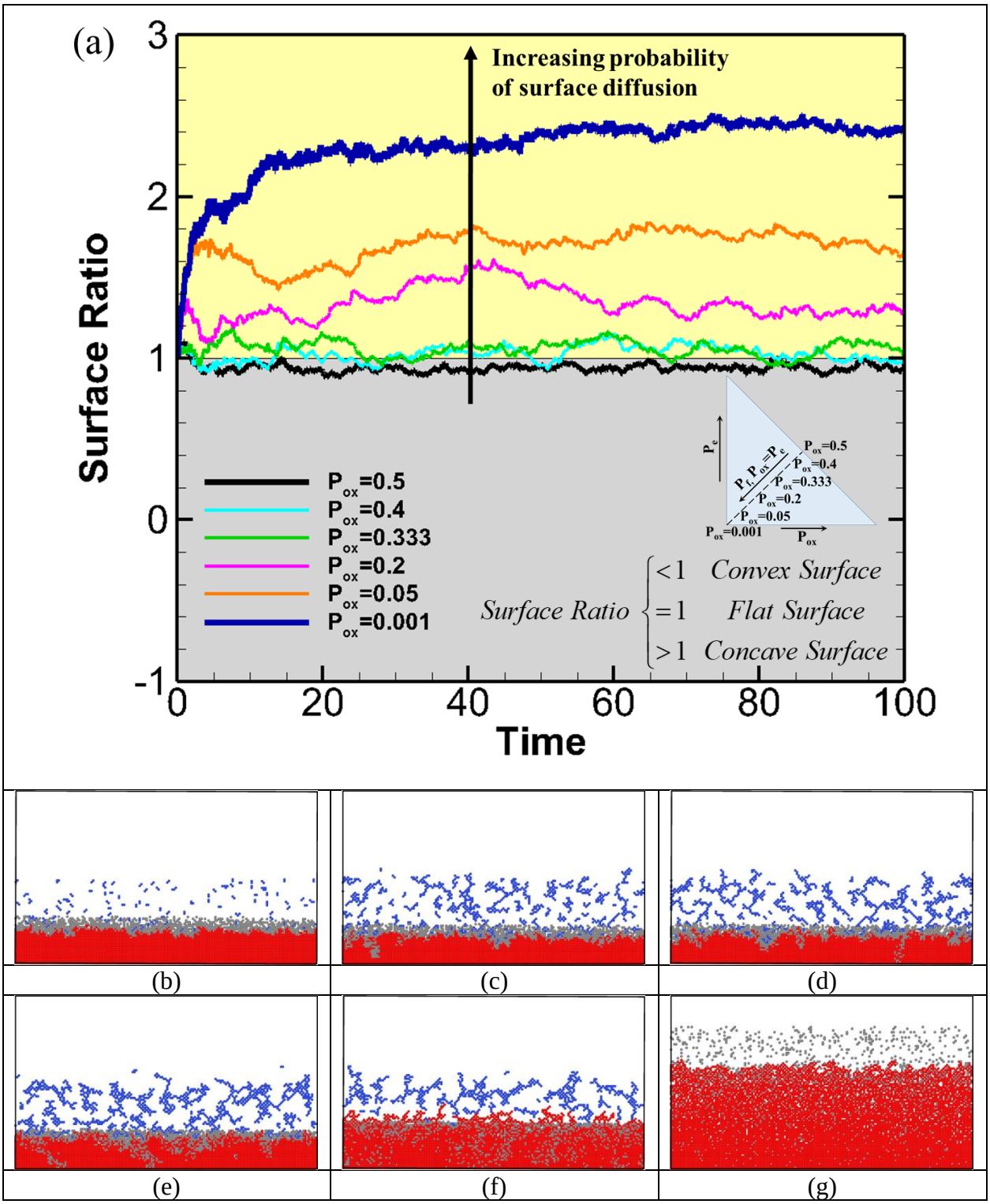

Figure 13: Evolution of the electrodissoluted surface with time for $P_{ox}=P_e$ and $P_f=1-2\times P_{ox}$. (a) Surface ratio (b) Microstructure for $P_{ox}=P_e=0.5$ (c) Microstructure for $P_{ox}=P_e=0.4$ (d) Microstructure for $P_{ox}=P_e=0.333$ (e) Microstructure for $P_{ox}=P_e=0.2$ (f) Microstructure for $P_{ox}=P_e=0.05$ (g) Microstructure for $P_{ox}=P_e=0.001$

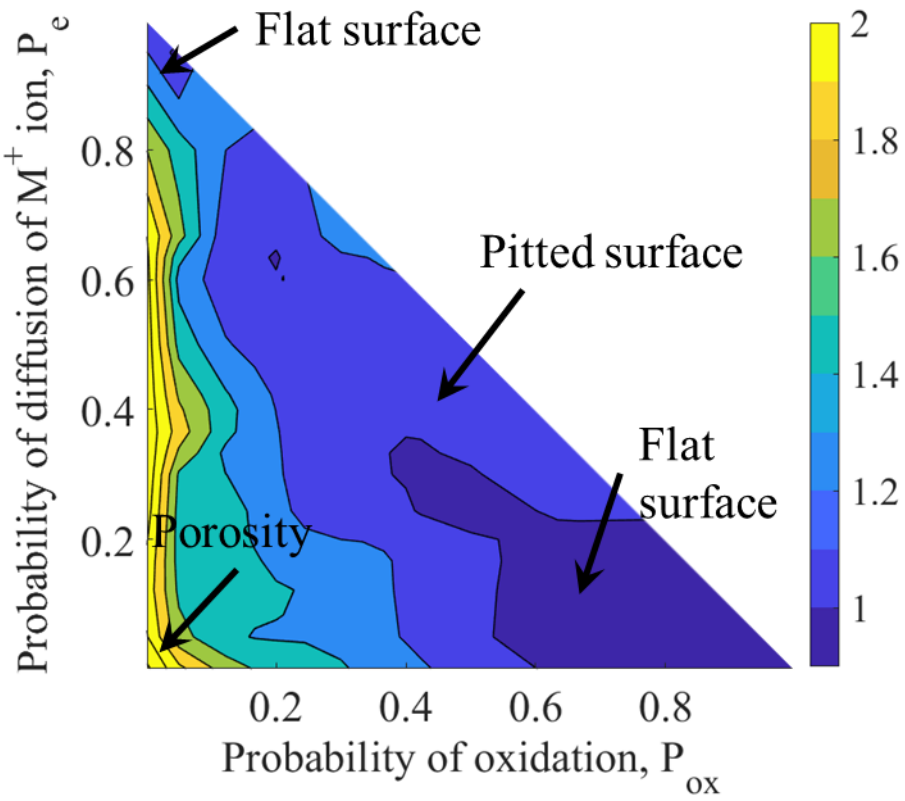

Figure 14: Contour of surface ratio of the interface between electrode and electrolyte with respect to probability of reduction, P_{ox} and probability of diffusion of M^+ ion in electrolyte, P_e at time = 100

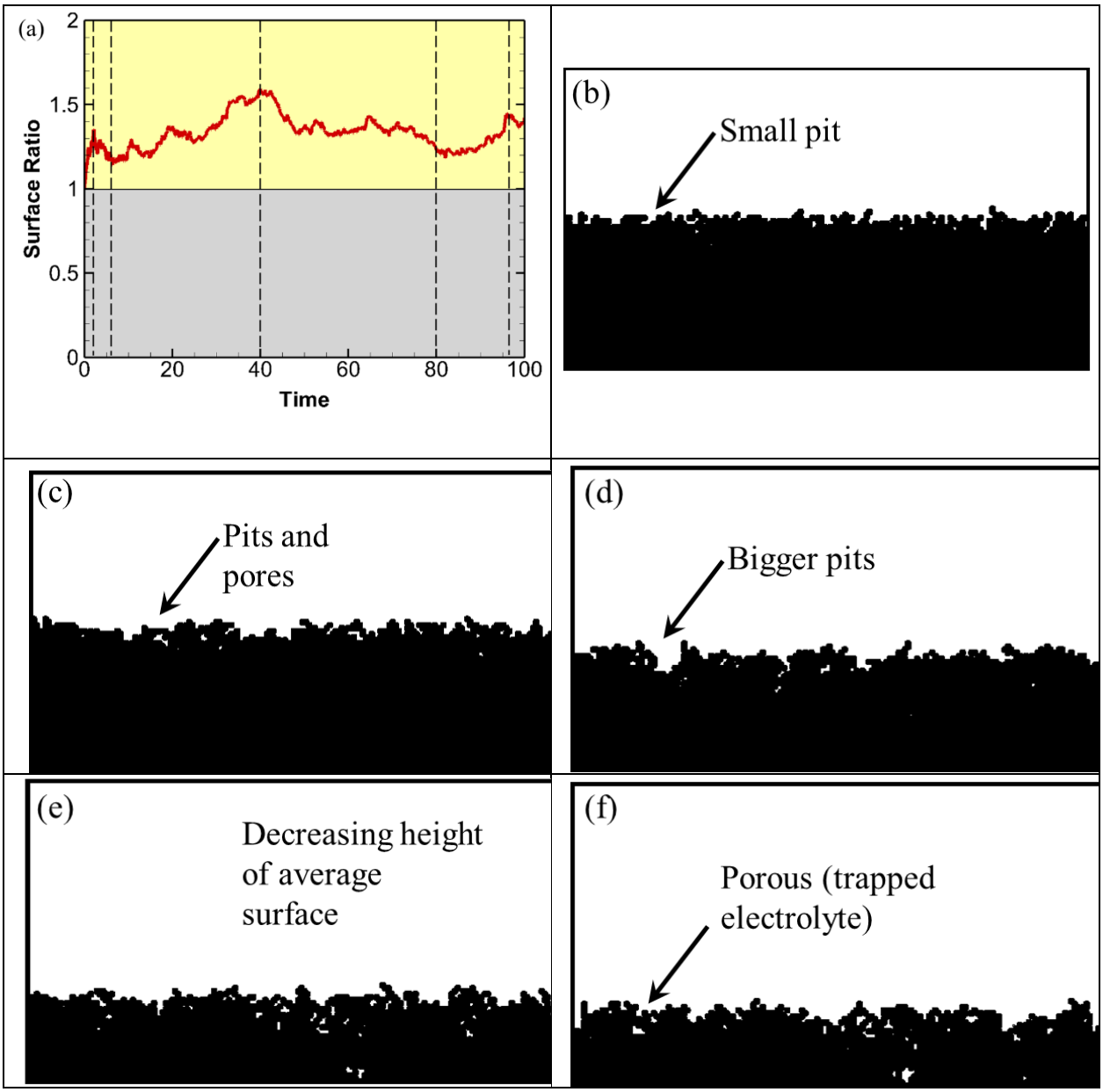

Figure 15: Evolution of surface ratio of the interface between electrode and electrolyte for P_{ox}=0.211, P_e=0.122 and P_f=0.667. (a) Surface ratio as function of time (b) Microstructure at time=4 (c) Microstructure at time=8 (d) Microstructure at time=40 (e) Microstructure at time=80 (f) Microstructure at time=92

Evolution of surface formed at the interface between electrode and electrolyte

In Figure 12, the surface ratio of the interface during electrodissolution and the corresponding microstructure is shown when there is no surface diffusion. The inset picture in Figure 12 (a) shows that value of P_{ox} ranging from 0.001 to 0.999 on the diagonal line with no surface diffusion. The value of P_e varies from 0.999 to 0.001. In figure 12 (a), the surface ratio the surface ratio for three curves for P_{ox}=0.8, 0.5 and 0.2 fluctuate because the rate of oxidation is high and when some dead metal is detached the value of surface ratio changes suddenly. The average surface ratio is about 0.95 for these curves. When P_{ox} is 0.001, there are very few oxidations and the surface ratio increases linearly from 1 to 1.05. When P_{ox} is 0.999, the surface ratio is nearly 1. Discharging along the diagonal line where the probability of surface diffusion is zero, the surface ratio is close to 1 and the interface is flat or nearly flat with small pits as seen in Figure 12 (b) to (f).

Figure 13 shows the evolution of surface ratio for equal probability of reduction and ion diffusion (P_{ox}=P_e) and the corresponding morphology. Surface diffusion increases from 0 at P_{ox}=0.5 to 0.998 at P_{ox}=0.001. The inset picture in Figure 13 (a) shows the values of P_{ox} used on the P_{ox}=P_e line. The interface between electrode and electrolyte is nearly flat when P_{ox}=0.5 during the entire duration of discharge. As the P_{ox} decreases and P_f increases, the value of surface ratio increases. Looking at microstructure in (b) to (e), the depth of pitting as well as trapped electrolyte has increased as the probability of surface diffusion has increased. In (f), whisker like features can be seen above the average interface with a porosity and trapped electrolyte. This is due to large probability of surface diffusion and slow oxidation and ion diffusion. In (g), when the surface diffusion is 0.998 while P_{ox} and P_e are orders of magnitude lower, the microstructure evolves to a very porous structure. One important point to note is that surface ratio evolves to a steady value after some initial time.

The contour of surface ratio of the interface between electrode and electrolyte with probability of oxidation, P_{ox} and probability of ion diffusion, P_e is shown in Figure 14. Across the entire space, the value of surface ratio is close to 1 or higher than 1 indicating that the interface contains pits or in the case of low P_{ox} and about 10^3 times P_f, a very porous microstructure. Flat interface is obtained in two regions, one where $P_{ox}>>P_e$ and P_f is close to zero and in the other region, $P_e>>P_{ox}$ and P_f is close to zero. Interface with pits is obtained when oxidation, ion diffusion and surface diffusion are equally.

Figure 15 shows the evolution of surface ratio of the interface for $P_{ox}=0.211$, $P_e=0.122$ and $P_f=0.667$ (this point lies on 30-degree line with respect to P_{ox} axis) and the corresponding microstructure. The surface ratio is always greater than one. The surface ratio is characterized by a series of minima and maxima. Figure 15 (b) correspond the maxima peak at time=4. During the start of discharge, as the first few layers are oxidized, small pits are formed and they occur frequently on the surface. Figure 15 (c) corresponds to the microstructure at the minima of surface ratio at time=8. The surface is characterized by pores and deeper pits than before, however the frequency of the pits is smaller than (b). Figure (d) corresponds to the maximum in surface ratio at time=40. The pits are now deeper and wider. Figure (e) corresponds to the minima in surface ratio at time=80. The surface is not as deeply pitted as before, but there are many pores just below the interface. Figure (f) corresponds to the maxima in surface ratio at time=92. The network of pores has been reduced compared to the previous microstructure. The amount of electrolyte trapped has increased with the progression of discharge.

An important thing to note is that the pits during discharging do not get deeper and deeper with progression of discharge. The diffusion of ions is restricted in a pit and they act as passivating layer, preventing further oxidation. This facilitates the oxidation of the top layer of the interface.

This process leads to a leveling effect during discharge and the height of the average surface decreases steadily. This is similar to the global or bulk dissolution of crystal in which overall height of the crystal is reduced along with the formation of pits [14].

Charge and Discharge

It is important to note that the rate at which number of layers are dissolved is faster during discharging than the rate at which number of layers are deposited during charging. This effect is specially marked when probability of reaction (either oxidation or reduction) and probability of ion diffusion is commensurate. During charging, the deposition is constrained by the arrival of ion at the interface, which is slow because of two factors, concentration of ions (about ten percent of lattice sites are occupied by ions and probability of diffusion of ions is less than one. During discharge, the only restriction on dissolution of the first layer is the assigned probability of oxidation. After that if the ions at the interface diffuse away, the next series of oxidations can occur. Therefore, the limit is on or two hops of the ions away from the interface for discharging while several hops are of ions towards the interface are required for charging process. This is consistent with the different time scales observed during charging and discharging[40].

For safe and efficient operation of battery, during charging uniform deposition is desirable and during discharging, minimum amount of dead metal would be preferable. For charging, this would imply restricting the battery operation to a limited range of P_{red} and P_e ($P_{red}<<P_e$). For discharging, there are two regions in which fewer dead metal per oxidation reaction is formed as seen in Figure 11 (c). In one region, $P_{ox}<<P_e$ and surface diffusion is very close to zero. In the other region, $P_{ox}>>P_e$ and surface diffusion is close to zero. The size of the second region is bigger than region one. In electrochemical systems like batteries, the probabilities can be adjusted by changing the overpotential during charging or discharging. Therefore, during charging, small overpotential and

therefore small P_{red} is recommended. During discharging, high overpotential and thus high P_{ox} would be preferable because the associated region seen in Figure 11 (c) is larger. Arakawa *et al.*[42] observed improved performance of lithium metal anode when discharging at high current density. Yoon et al [23] report that formation of dead lithium is facilitated if the lithium electrode is discharged at low current density using a continuum mechanics formulation.

Batteries also entail cycling of charge and discharge processes. In this study, at the start of charging and discharging, the interface was flat. In the scenario, that charging happens first and then discharging, if the morphology is mossy or dendritic deposition, more dead metal will be formed because there are many arrangements in which a cluster of atoms is connected to the substrate through a linchpin atom. If this particular linchpin atom is oxidized, the cluster of atoms are separated from electrode and are counted as dead metal. If discharge occurs first and then charge, if there is dead metal near the electrode, the mass transport of ions near the electrode will be reduced because the dead metal will act as obstacle to ion diffusion. Smaller ion diffusion would lead to dendritic deposition.

Conclusions

A wide range of microstructure during charging process, needles, whiskers, mossy, dendrite, non-uniform and uniform deposition depending upon the combination of probability of reduction, ion diffusion in electrolyte or surface diffusion on metallic surface. In contrast, during discharging, the microstructure is either porous for large surface diffusion, pitted or pitted with trapped electrolyte. During charging, the number of layers deposited, and the average height of the deposition can increase very sharply when P_{red} and P_e are similar in value. During discharging, the number of layers dissolved increases linearly with time.

The surface ratio of the interface between electrode and electrolyte has a crossover during charging. During the initial phase of charging, the surface ratio is less than one for the entire P_{red}-P_e space. However, for $P_{red}<<P_e$, the surface ratio becomes greater than or equal to one with the progression of the charging process. In the rest of the P_{red}-P_e space, the surface ratio is less than one. For discharging, the surface ratio is about one when surface diffusion is not allowed, or greater than one for the entire P_{ox}-P_e range. The nature of the interface is either flat surface or convex surface depending upon P_{red} and P_e combination during charging while during discharging, the interface can be approximated as concave surface. The surface ratio evolve to a steady value during both charging and discharging and can be useful in updating the surface activity in reaction rates during continuum studies.

Surface diffusion is key in determining the morphology during charging. High surface diffusion and low reduction results in whiskers and comparable surface diffusion and reduction result in mossy deposition. During discharging, higher surface diffusion results in greater amount of dead metal.

Supporting Information

The details of the mesoscale KMC algorithm used for charging and discharging is provided in the supporting information document. The effect of computational domain on KMC solution for both charging and discharging is included in the supporting information.

Acknowledgement

The information, data, or work presented herein was funded in part by the Office of Energy Efficiency and Renewable Energy (EERE), U.S. Department of Energy, under Award DE-

EE0007766. Support also in part from Purdue University's College of Engineering Data Science Initiative Seed Funding is gratefully acknowledged.

References

(1) Barton, J. L.; Bockris, J. O. The Electrolytic Growth of Dendrites from Ionic Solutions. *Proc. R. Soc. A Math. Phys. Eng. Sci.* **1962**, *268* (1335), 485–505.

(2) Diggle, J. W.; Despic, A. R.; Bockris, J. O. The Mechanism of the Dendritic Electrocrystallization of Zinc. *J. Electrochem. Soc.* **1969**, *116* (11), 1503.

(3) Monroe, C.; Newman, J. Dendrite Growth in Lithium/Polymer Systems. *J. Electrochem. Soc.* **2003**, *150* (10), A1377.

(4) Monroe, C.; Newman, J. The Effect of Interfacial Deformation on Electrodeposition Kinetics. *J. Electrochem. Soc.* **2004**, *151* (6), A880.

(5) Chen, L.; Zhang, H. W.; Liang, L. Y.; Liu, Z.; Qi, Y.; Lu, P.; Chen, J.; Chen, L.-Q. Modulation of Dendritic Patterns during Electrodeposition: A Nonlinear Phase-Field Model. *J. Power Sources* **2015**, *300*, 376–385.

(6) McCoy, J. M.; LaFemina, J. P. Kinetic Monte Carlo Investigation of Pit Formation at the CaCO3(10$\bar{1}$4) Surface-Water Interface. *Surf. Sci.* **1997**, *373* (2–3), 288–299.

(7) Wehrli, B. Monte Carlo Simulations of Surface Morphologies during Mineral Dissolution. **1989**, *132* (1), 230–242.

(8) Kurganskaya, I.; Luttge, A. A Comprehensive Stochastic Model of Phyllosilicate Dissolution: Structure and Kinematics of Etch Pits Formed on Muscovite Basal Face. *Geochim. Cosmochim. Acta* **2013**, *120*, 545–560.

(9) Fischer, C.; Kurganskaya, I.; Luttge, A. Inherited Control of Crystal Surface Reactivity. *Appl. Geochemistry* **2018**, *91* (February), 140–148.

(10) Meakin, P.; Rosso, K. M. Simple Kinetic Monte Carlo Models for Dissolution Pitting Induced by Crystal Defects. *J. Chem. Phys.* **2008**, *129* (20), 204106.

(11) Lillard, R. S.; Wang, G. F.; Baskes, M. I. The Role of Metallic Bonding in the Crystallographic Pitting of Magnesium. *J. Electrochem. Soc.* **2006**, *153* (9), B358.

(12) Gosalvez, M. A.; Nieminen, R. M.; Kilpinen, P.; Haimi, E.; Lindroos, V. Anisotropic Wet Chemical Etching of Crystalline Silicon: Atomistic Monte-Carlo Simulations and Experiments. *Appl. Surf. Sci.* **2001**, *178* (1–4), 7–26.

(13) Gupta, A.; Aldinger, B. S.; Faggin, M. F.; Hines, M. A. Kinetic Monte Carlo Simulations of Anisotropic Si(100) Etching: Modeling the Chemical Origins of Characteristic Etch Morphologies. *J. Chem. Phys.* **2010**, *133* (4).

(14) Lasaga, A.; L\"uttge, A. Variation of Crystal Dissolution Rate Based on a Dissolution Step

Wave Model. *Science (80-.).* **2001**, *291* (March), 2400–2404.

(15) Kushima, A.; So, K. P.; Su, C.; Bai, P.; Kuriyama, N.; Maebashi, T.; Fujiwara, Y.; Bazant, M. Z.; Li, J. Liquid Cell Transmission Electron Microscopy Observation of Lithium Metal Growth and Dissolution: Root Growth, Dead Lithium and Lithium Flotsams. *Nano Energy* **2017**, *32* (December 2016), 271–279.

(16) Steiger, J.; Kramer, D.; Mönig, R. Microscopic Observations of the Formation, Growth and Shrinkage of Lithium Moss during Electrodeposition and Dissolution. *Electrochim. Acta* **2014**, *136*, 529–536.

(17) Bai, P.; Li, J.; Brushett, F. R.; Bazant, M. Z. Transition of Lithium Growth Mechanisms in Liquid Electrolytes. *Energy Environ. Sci.* **2016**, *9* (10), 3221–3229.

(18) Gireaud, L.; Grugeon, S.; Laruelle, S.; Yrieix, B.; Tarascon, J. M. Lithium Metal Stripping/Plating Mechanisms Studies: A Metallurgical Approach. *Electrochem. commun.* **2006**, *8* (10), 1639–1649.

(19) Wood, K. N.; Kazyak, E.; Chadwick, A. F.; Chen, K.-H.; Zhang, J.-G.; Thornton, K.; Dasgupta, N. P. Dendrites and Pits: Untangling the Complex Behavior of Lithium Metal Anodes through Operando Video Microscopy.

(20) Chen, K.-H.; Wood, K. N.; Kazyak, E.; LePage, W. S.; Davis, A. L.; Sanchez, A. J.; Dasgupta, N. P. Dead Lithium: Mass Transport Effects on Voltage, Capacity, and Failure of Lithium Metal Anodes. *J. Mater. Chem. A* **2017**, *5* (23), 11671–11681.

(21) Wood, K. N.; Noked, M.; Dasgupta, N. P. Lithium Metal Anodes: Toward an Improved Understanding of Coupled Morphological, Electrochemical, and Mechanical Behavior. *ACS Energy Lett.* **2017**, *2* (3), 664–672.

(22) Aryanfar, A.; Brooks, D. J.; Colussi, A. J.; Hoffmann, M. R. Quantifying the Dependence of Dead Lithium Losses on the Cycling Period in Lithium Metal Batteries. *Phys. Chem. Chem. Phys.* **2014**, *16* (45), 24965–24970.

(23) Yoon, G.; Moon, S.; Ceder, G.; Kang, K. Deposition and Stripping Behavior of Lithium Metal in Electrochemical System: Continuum Mechanics Study. *Chem. Mater.* **2018**, acs.chemmater.8b02623.

(24) Shvab, I.; Brochard, L.; Manzano, H.; Masoero, E. Precipitation Mechanisms of Mesoporous Nanoparticle Aggregates: Off-Lattice, Coarse-Grained, Kinetic Simulations. *Cryst. Growth Des.* **2017**, *17* (3), 1316–1327.

(25) Trigueros, P. P.; Mas, F.; Claret, J.; Sagués, F.; Galceran, J.; Puy, J. Monte Carlo Simulation of Diffusion-Controlled Response Functions at 2D Experimental Rough Electrodes. *J. Electroanal. Chem.* **1993**, *348* (1–2), 221–246.

(26) Guo, L.; Radisic, A.; Searson, P. C. Kinetic Monte Carlo Simulations of Nucleation and Growth in Electrodeposition. *J. Phys. Chem. B* **2005**, *109* (50), 24008–24015.

(27) Drews, T. O.; Ganley, J. C.; Alkire, R. C. Evolution of Surface Roughness during Copper Electrodeposition in the Presence of Additives. *J. Electrochem. Soc.* **2003**, *150* (5), C325.

(28) Liu, J.; Liu, C.; Conway, P. P. Kinetic Monte Carlo Simulation of Kinetically Limited Copper Electrocrystallization on an Atomically Even Surface. *Electrochim. Acta* **2009**, *54* (27), 6941–6948.

(29) Tewari, D.; Liu, Z.; Balbuena, P. B.; Mukherjee, P. P. Mesoscale Understanding of Lithium Electrodeposition for Intercalation Electrodes. *J. Phys. Chem. C* **2018**, *122*, 21097–21107.

(30) Hao, F.; Mukherjee, P. P. Mesoscale Analysis of the Electrolyte-Electrode Interface in All-Solid-State Li-Ion Batteries. *J. Electrochem. Soc.* **2018**, *165* (9), A1857–A1864.

(31) Hao, F.; Verma, A.; Mukherjee, P. P. Mesoscale Complexations in Lithium Electrodeposition. *ACS Appl. Mater. Interfaces* **2018**, *10* (31), 26320–26327.

(32) Hao, F.; Verma, A.; Mukherjee, P. P. Mechanistic Insight into Dendrite–SEI Interactions for Lithium Metal Electrodes. *J. Mater. Chem. A* **2018**, 19664–19671.

(33) Haldar, P.; Chatterjee, A. Connectivity-List Based Characterization of 3D Nanoporous Structures Formed via Selective Dissolution. *Acta Mater.* **2017**, *127*, 379–388.

(34) Erlebacher, J.; Aziz, M. J.; Karma, A.; Dimitrov, N.; Sieradzki, K. Evolution of Nanoporosity in Dealloying. *Nature* **2001**, *410* (6827), 450–453.

(35) Córdoba-Torres, P. Chemical Ordering and Kinetic Roughening at Metal-Electrolyte Interfaces. *Phys. Rev. B - Condens. Matter Mater. Phys.* **2007**, *75* (11), 1–13.

(36) Lüttge, A.; Arvidson, R. S.; Fischer, C. A Stochastic Treatment of Crystal Dissolution Kinetics. *Elements* **2013**, *9* (3), 183–188.

(37) Douglass, I.; Harrowell, P. Kinetics of Dissolution of an Amorphous Solid. *J. Phys. Chem. B* **2018**, *122* (8), 2425–2433.

(38) Quiroga, M. A.; Franco, A. A. A Multi-Paradigm Computational Model of Materials Electrochemical Reactivity for Energy Conversion and Storage. *J. Electrochem. Soc.* **2015**, *162* (7), E73–E83.

(39) Röder, F.; Braatz, R. D.; Krewer, U. Multi-Scale Simulation of Heterogeneous Surface Film Growth Mechanisms in Lithium-Ion Batteries. *J. Electrochem. Soc.* **2017**, *164* (11), E3335–E3344.

(40) Saedi, A. A Study on Mutual Interaction between Atomistic and Macroscopic Phenomena during Electrochemical Processes Using Coupled Finite Difference - Kinetic Monte Carlo Model: Application to Potential Step Test in Simple Copper Sulfate Bath. *J. Electroanal. Chem.* **2006**, *588* (2), 267–284.

(41) Schwarzacher, W. Electrodeposition: A Technology for the Future. *Electrochem. Soc. Interface* **2006**, *15* (1), 32–35.

(42) Arakawa, M.; Tobishima, S. ichi; Nemoto, Y.; Ichimura, M.; Yamaki, J. ichi. Lithium Electrode Cycleability and Morphology Dependence on Current Density. *J. Power Sources* **1993**, *43* (1–3), 27–35.

(43) Langenhuizen, N. P. W. The Effect of Mass Transport on Li Deposition and Dissolution. *J. Electrochem. Soc.* **1998**, *145* (9), 3094–3099.

(44) Wood, K. N.; Kazyak, E.; Chadwick, A. F.; Chen, K. H.; Zhang, J. G.; Thornton, K.; Dasgupta, N. P. Dendrites and Pits: Untangling the Complex Behavior of Lithium Metal Anodes through Operando Video Microscopy. *ACS Cent. Sci.* **2016**, *2* (11), 790–801.

(45) Yoshimatsu, I.; Hirai, T.; Yamaki, J. Lithium Electrode Morphology during Cycling in Lithium Cells. *J. Electrochem. Soc.* **1988**, *135* (10), 2422.

TOC Graphics

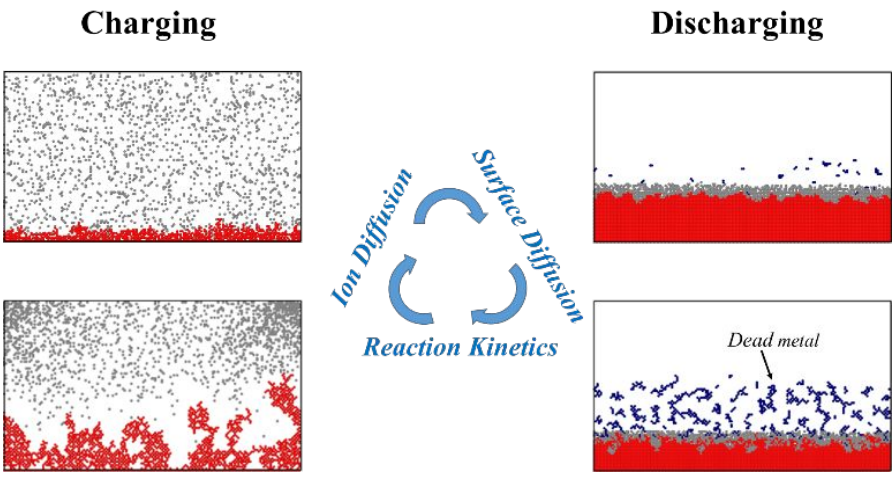

Mechanisms driving the evolution of metal electrode interface during plating and stripping and formation of dead metal.